0

UNITED STATES ATOMIC ENERGY COMMISSION

UCRL-2441

HIGH ENERGY (d,p) REACTIONS (Thesis)

By
Louis Maurice Slater

March 1954

Radiation Laboratory
University of California
Berkeley 4, California

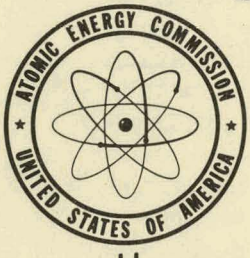

Technical Information Service, Oak Ridge, Tennessee

DISCLAIMER

TABLE OF CONTENTS

Subject Category, PHYSICS.
Work performed under Contract No. W-7405-eng-48.

Printed in USA, Price 60 cents. Available from the Office of Technical Services, Department of Commerce, Washington 25, D. C.

AEC, Oak Ridge, Tenn.-W42312

PAGES 3 to 4

WERE INTENTIONALLY

LEFT BLANK

2

High Energy (d,p) Reactions

Louis Maurice Slater
Department of Chemistry and Radiation Laboratory
University of California, Berkeley, California

ABSTRACT

Excitation functions for the (d,p) reaction on U^{238} and Th^{232} and for the (d,n) reactions on Th^{232} have been run in the energy range of the deuterons of the Berkeley 60-inch cyclotron. Excitation functions for the (d,p) reaction on U^{238}, Th^{232}, Pt^{198}, Pd^{110}, Zr^{96}, and Mn^{55} have also been run in the energy range of the deuterons of the Berkeley 184-inch cyclotron. The experimentally observed high-energy (d,p) excitation functions all exhibit remarkably similar absolute cross-section values.

Recent experimental and theoretical work on total nuclear cross sections for neutron capture together with the success of the shell model of nuclear structure suggests that a nucleon entering the nucleus from the outside, to some extent will move like an independent particle in a potential trough and interact relatively weakly with the other nucleons.

Calculations were made to determine available vacancies for neutron capture to bound levels corresponding to those of a "particle in a box." A spherical potential well was assumed for the nucleus with dimensions corresponding to those calculated for the various nuclei studied. The number of available neutron vacancies was shown to be similar for all of the nuclei studied, thus lending support to the proposed model.

Additional support for the model was furnished by the experimentally observed greater cross-section values for the formation of Pd^{111g} than for the formation of higher spin valued Pd^{111m} in the (d,p) reaction on Pd^{110}. It was shown that previous work on the high energy $Bi^{209}(d,p)Bi^{210}$ (RaE) excitation function was not a variance with the proposed model; in fact, lower cross-section values for the formation of RaE than for the isotopes studied here were to be expected.

High Energy (d,p) Reactions

Louis Maurice Slater
Department of Chemistry and Radiation Laboratory
University of California, Berkeley, California

March, 1954

A. INTRODUCTION

The Oppenheimer-Phillips or "stripping" reaction[1] has been known for some time. Included in this general type of reaction are the (d,p) and (d,n) reactions. Related to these are the inverse or "pick-up" reactions such as (p,d) and (n,d). Experimentally the (d,p) reaction has been studied more than the (d,n) reaction. Spectra and angular distribution of protons resulting from the (d,p) reaction have been studied experimentally. Differential cross section as a function of angle has been treated theoretically for the "stripping" and "pick-up" processes by various investigators. However, total or integrated cross sections for the (d,p) reaction and especially for the (d,n) reaction have been rather neglected experimentally and theoretically by investigators.

Where total cross section values for the "stripping" reaction have been studied experimentally, the energy of the deuterons used usually varied from zero to not more than 20 Mev. The only exception to this is the $Bi^{209}(d,p)Bi^{210}$ excitation function as studied by Si-Chang Fung.[2] He employed deuterons ranging in energy from 40 to 190 Mev in an extension of the $Bi^{204}(d,p)Bi^{210}$ excitation function as studied by Kelly and Segrè[3] for deuterons of energy 20 Mev and lower. However, in actuality the total (d,p) excitation function was not measured for only RaE was observed. Because of it's great half-life, the other isomer of Bi^{210} was not observed.

Because of the availability of thin foils of uranium and thorium, excitation functions for the reactions $U^{238}(d,p)U^{239}$ and $Th^{232}(d,p)Th^{233}$ were run for deuterons of energy up to 20 Mev by bombardments on the Berkeley 60-inch cyclotron. Because the yield of Th^{233} was determined from the activity of its daughter Pa^{233}, the sum of the $Th^{232}(d,p)Th^{233}$ and $Th^{233}(d,n)Pa^{233}$ excitation functions was also easily obtained by not scavenging for initially formed protactinium. The $Th^{232}(d,n)Pa^{233}$ excitation function was obtained by difference.

The $U^{238}(d,p)U^{239}$ and $Th^{232}(d,p)Th^{233}$ excitation functions were extended by deuteron runs made on uranium and thorium using the deuterons of the Berkeley 184-inch cyclotron which have a maximum energy of 195 Mev. Comparison of the resulting (d,p) excitation functions with that on Bi^{209} showed that the latter was considerably lower in magnitude and fell off much more sharply with increasing deuteron energy. It was suspected that perhaps the reason for this discrepancy was related to the fact that Bi^{210} was one neutron and one proton beyond major closed shells.

Because of the lack of experimental work on high energy (d,p) reactions and in the hope of explaining the discrepancy noted above as well as obtaining a general explanation of total "stripping" reaction cross section values, it was decided to study additional high-energy (d,p) reactions. Study of high-energy (d,p) reactions is generally easier than study of the corresponding low-energy reactions because of the difficulty in obtaining pure uniform foils of about 1 mil in thickness necessary for low-energy deuteron reactions. Foils much greater than 1 mil in thickness cause too large a degradation of deuteron energy in the region of 20 Mev or less. Also, the "stripping"

reaction excitation functions in the high-energy region are quite smooth compared to the region near the peak. This results in the need for fewer experimental points to fix the excitation function in the high-energy deuteron region.

The choice of target materials for study of high-energy (d,p) reactions by chemical separation is rather severely limited. First the target material must be available in the form of a metallic foil of fairly high melting point and very high purity. It is very difficult to prepare powder targets of sufficient durability, thinness, and uniformity for use in these experiments. The isotope resulting from the (d,p) reaction must have a reasonably long half-life to enable chemical separation from contaminating activities. It is to be noted that where high-energy deuterons are employed the (d,p) reaction can only be studied on the heaviest isotope of a particular element if there are two or more isotopes in the target material. The highter cross-section valued (d,dxn) reactions on the heaviest isotope would result in the same products as (d,p) reactions on lighter isotopes. Therefore all (d,p) reactions reported below have been corrected for isotopic abundance as given in the Table of Isotopes.[4] The smaller the abundance of the heaviest isotope of an element, the harder it is to experimentally observe the (d,p) reaction. Unless the isotope resulting from the (d,p) reaction has a radioactive daughter of reasonable half-life, its half-life should be unique among the half-lives of activities produced by (d,dxn) reactions on the various isotopes in the target element. (d,p) cross section values are quite small for high-energy deuterons, and activities with comparable half-life make very difficult or impossible the detection of the product activity of the (d,p) reaction.

Because of the above considerations, successful study of high energy (d,p) reactions were limited to the following cases:

$$U^{238}(d,p)U^{239}$$
$$Th^{232}(d,p)Th^{233}$$
$$Pt^{198}(d,p)Pt^{199}$$
$$Pd^{110}(d,p)Pd^{111g},Pd^{111m}$$
$$Zr^{96}(d,p)Zr^{97}$$
$$Mn^{55}(d,p)Mn^{56} .$$

The only case studied near a closed shell is that of $Pd^{110}(d,p)Pd^{111g} + Pd^{111m}$. The $_{65}Pd^{111}$ is one neutron past the closed sub-shell of 64 neutrons. However, in the model described in the discussion, effects caused by closed shells would be taken into account by the accompanying changes in such general parameters as the nuclear radius and binding energy.

B. EXPERIMENTAL PROCEDURES

1. Target preparation.--Uranium discs of 1 mil and 0.5 mil thickness and thorium discs of 1 mil thickness were cut from sheet uranium and thorium with a 1 inch diameter steel die. These were checked for uniformity of thickness with a micrometer and discs varying more than ±5 percent in thickness were rejected. Those remaining were accurately weighed and stacks of these foils served as targets for the deuterons of the Berkeley 60-inch cyclotron. The foils were mounted at the end of a Faraday cup with a 3/4 inch opening. They were secured by a cap with a 3/4 inch opening. In this arrangement and with the cyclotron

port used the maximum energy of the 1/8 inch collimated beam of deuterons striking the first target was 20.2 ± 0.2 Mev. In the case of uranium the number of foils that could be worked up simultaneously was limited to six because of the 23.54 minute half-life of U^{239}. Therefore, 5 mil discs of uranium were placed in front of the target foils to degrade the deuteron energy in studying various regions of the excitation function.

Targets for the deuterons of the Berkeley 184-inch synchrocyclotron were usually made from 1 inch discs of 5-10 mil thickness. These were also checked for uniformity of thickness and accurately weighed. Two aluminum foils, 1 inch in diameter, of 0.5-1 mil thickness, accurately weighed, were glued at opposite edges to the target discs, one on each side. The resulting foil stack was cut in two. One to one and one-half mil thick aluminum guard foils were inserted between the target foil and the two aluminum monitors. The whole assembly was covered with another guard foil of aluminum. A standard "clothes-pin" type target holder was used for mounting.

The manganese metal used was too brittle to cut into discs with a die. It had been produced by electrodeposition and one side was very smooth while the other was quite granular. Rectangular pieces were formed by scoring the smooth surface with a diamond stylus and breaking. Pieces were chosen with small and uniform granulations on the rough surface. Only one aluminum monitor foil was used because of the roughness of one surface. Guard foils were used between the monitor and the target as well as around the whole assembly. Because of the brittleness of the manganese, enhanced by a small amount of hydrogen impurity, the target could not be cut after bombardment. Hence, since the whole of the manganese target was destined to be worked up, only

an extension of the outer aluminum guard foil was secured by the jaws of the "clothes-pin" type target holder. This was to ensure that all of the deuterons striking the manganese were of the same energy; that is, the jaws of the target holder would not cause any degradation of the energy of the deuterons striking the target.

2. Bombardment procedures.--For deuteron bombardments using the 60-inch cyclotron the use of an aluminum monitor was impractical. The $Al^{27}(d,\alpha p)Na^{24}$ excitation function rises much too rapidly in the vicinity of 20 Mev. The deuteron beam was monitored by recording current integrators. A "beam profile" was also taken by means of a "Speedomax" recording device. Both of these instruments were calibrated before and sometimes after runs by means of an accurately known false beam. The effect of secondary electrons from the target was negligible because of the fringing of the magnetic field at the position of the Faraday cup. Preliminary runs were always made with a strip of cellulose tape replacing the target. These were done to ensure that the deuteron beam would strike the target and not the lip of the Faraday cup as well as to ascertain whether the deuteron beam was of sufficiently great intensity.

Bombardments varied from 5-20 minutes, depending upon beam intensity. The total number of deuterons delivered was obtained from the current integrators. This was checked by integration under the current profile with a planimeter. Correction for variation of the beam intensity during the bombardment was made by dividing the current profile into one minute intervals and integrating each of these with

a planimeter. The total current delivered in each interval was exponentially reduced, using the appropriate half-life, to the time of the end of the bombardment. The sum of the resulting "decayed" total currents represented the effective total current if delivered instantaneously at the time of the end of the bombardment.

The rate of deuteron energy degradation with thickness of thorium or uranium target as a function of deuteron energy is given in Figure 1. I am thankful to W. W. Crane for this graph. The rate of deuteron energy degradation is almost exactly the same for thorium and uranium. Figure 2 shows the energy of the deuterons, as a function of target thickness, as they are degraded from their initial energy of 20.2 Mev.

The energy of the deuterons striking the target in 184-inch cyclotron runs is a function of the radius of the target in the tank. Below 50 Mev, energy definition of the deuteron beam is quite poor. For this reason runs were made with deuterons of 50-190 Mev energy, usually at intervals of 50 Mev. The degradation of deuteron energy caused by target thickness was quite small.

The total number of deuterons striking the target in the 184-inch cyclotron runs was ascertained from the Na^{24} activity produced in the aluminum monitors and the known cross sections for the $Al^{27}(d,\alpha p)Na^{24}$ excitation function, as shown in Figure 3, courtesy of E. B. King and the California Research and Development Corporation. The effect of variation of beam intensity with time was avoided by bombarding for periods short compared to the half-life of the desired product isotope as well as by tuning up the cyclotron before the target was bombarded.

10

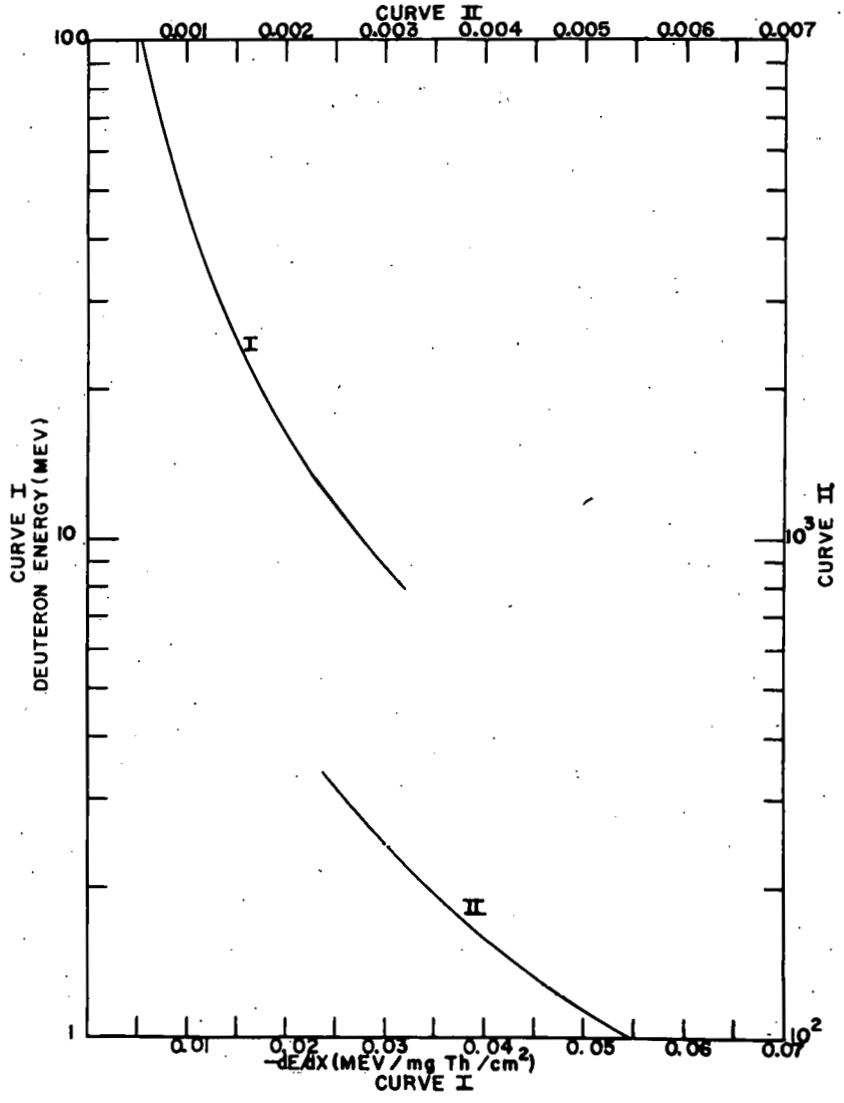

Fig. 1—Rate of energy loss of deuterons in thorium.

//

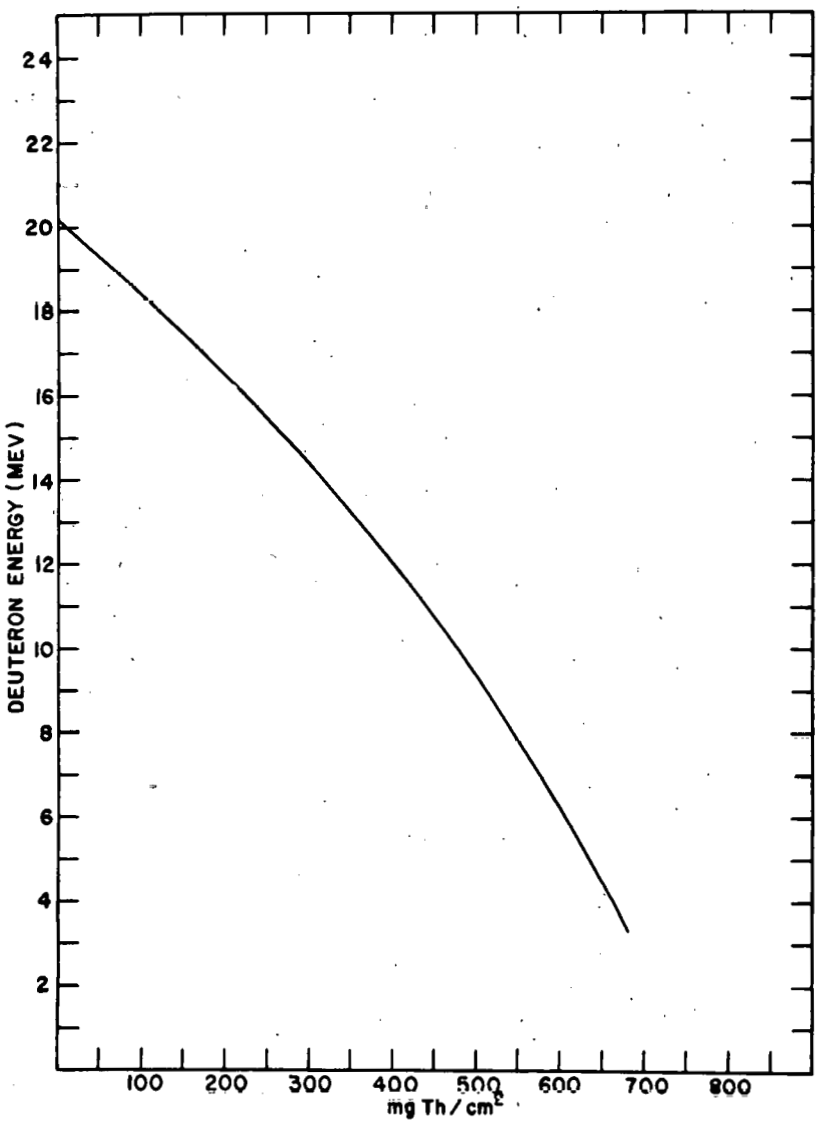

Fig. 2—Energy of deuterons of 20.2 Mev initial energy as a function of thorium target thickness.

12

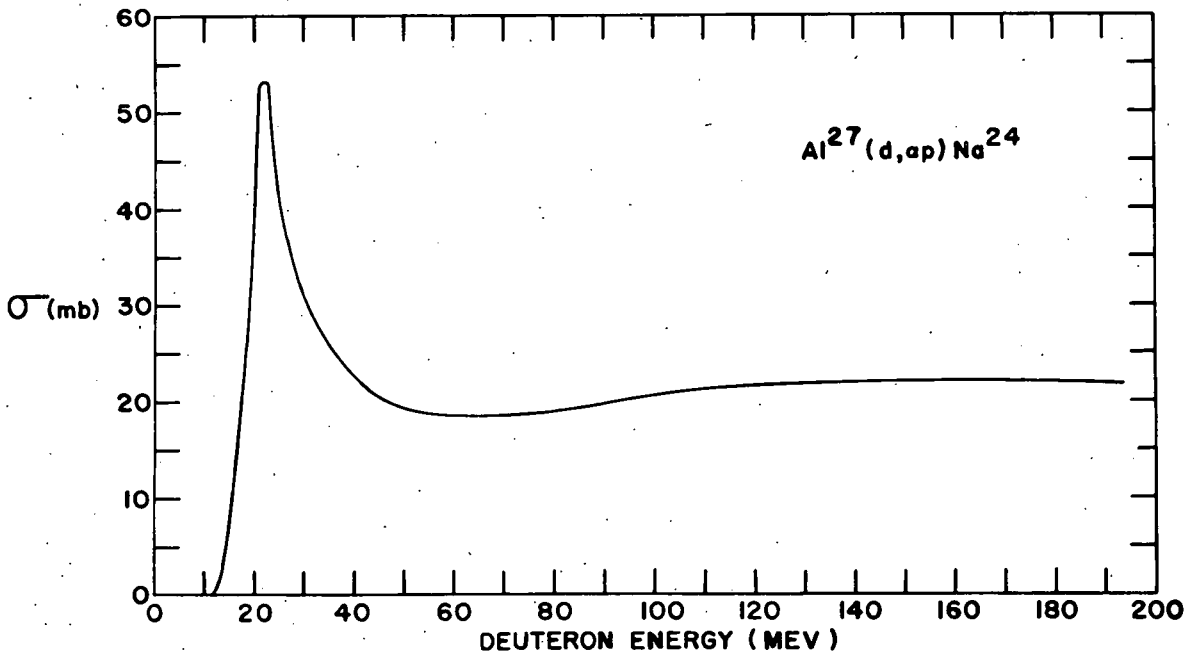

Fig. 3 — $Al^{27}(d,\alpha p)Na^{24}$ excitation function.

The beam of deuterons is depressed from the middle of the tank for energies below the maximum to about 100 Mev; below this it again rises somewhat. Because of this, for maximum production of activity, the target should be placed below the center of the target holder for energies other than the 195 Mev maximum.

3. Target handling procedures.--In the 60-inch cyclotron runs, the whole discs of uranium and thorium were dissolved and worked up. However, with the exception of manganese, strips of target a few millimeters wide were cut off after bombardment by deuterons of the 184-inch cyclotron. The guard foils and monitors were removed and the target strips weighed, dissolved, and worked up. Narrow strips were cut off because most of the target activity is produced near the edge and because it was desirable to have the area of the monitors counted as small as that of the final sample activity counted.

4. Counting procedures.--All Geiger activity was counted on the bottom of shelf two using chlorine-argon filled Amperex tubes with a window thickness of 3.5 milligrams of mica/cm^2. The total air-window thickness was 5.8 mg/cm^2. Alpha activity was counted on an argon filled windowless proportional counter. With the exception of thorium bombardments, all Geiger activity was counted using the same Geiger-Müeller tube and scaler. Weightless samples of protactinium mounted on platinum were counted on shelf two with a counter calibrated to within 10 percent for the beta particles of Pa^{233}. This was done by the California Research and Development Corporation by counting the

alpha activity of the daughter U^{233} of a large sample of Pa^{233}. The absolute geometry and counting efficiency of this counter on shelf two were also obtained by means of a 4π geometry counter. The absolute geometry and counting efficiency on shelf two of the counter used for the other beta activities encountered were obtained by comparison with the standardized counter. For all runs, except those on platinum and palladium, where aluminum monitors were used it was assumed that the same geometry and counting efficiency applied both to the sample activity and to the Na^{24} activity of the aluminum monitors. In the cases of platinum and palladium, where the final samples consisted of electrodeposits of gold and silver, respectively, a correction of 4 percent was used because of the 3/4 inch diameter of the samples. Other samples were usually mounted on platinum "hats" with the sample covering one square centimeter. This is about the same area as covered by the aluminum monitors; the monitors being mounted on saturated aluminum backscattering backing.

Air-window corrections for each beta activity encountered (including more than one in a sample) were made as follows:

$$\text{correction} = 1/\text{transmission} = 2^{5.8 \text{ mg /cm}^2/T_{1/2}},$$

where $T_{1/2}$ is the half-thickness in mg aluminum/cm^2 for the particular beta activity. For the 1.390 Mev beta particle of Na^{24}, this correction amounts to 5.15 percent.

Backscattering corrections are those of B. P. Burtt.[5] The saturated aluminum backscattering factor for beta particles of Na^{24} is 1.276. The saturated platinum backscattering factor for beta particles of approximately 0.6 Mev maximum energy or greater is 1.78.

Selfscattering corrections for sample thickness were obtained from data gathered by W. E. Nervik and P. C. Stevenson[6] as shown in Figures 4 and 5. Whenever practical, sample thicknesses were made such that the selfscattering corrections were found in the flat section of the curves. An attempt was also made to flatten and smooth out any unevenness in the samples. Samples were secured to the platinum "hats" with about 2 drops of zapon solution diluted approximately 4 to 1. The mass of the zapon was negligible in considering selfscattering corrections. Selfscattering corrections for monitor thickness are given by Figure 6, courtesy of E. B. King and the California Research and Development Corporation.

All correction factors, as well as necessary supplementary information such as sample thicknesses, not given above are to be found in section D, RESULTS. This is done to enable re-evaluation of the experimental data in the light of more accurate information, such as on selfscattering, as it becomes known.

C. CHEMICAL PROCEDURES

1. $U^{238}(d,p)U^{239}$.--The uranium target was dissolved in a small amount of concentrated HNO_3. About 20 ml of a solution 10 M in NH_4NO_3 (saturated) and 0.1 M in HNO_3 was added along with a small amount of solid NH_4NO_3. Approximately 30 ml of diethyl ether was added and the mixture was shaken in a 100 ml Kjeldahl flask. After separation of the phases the flask was immersed in a dry ice-acetone mixture until the aqueous phase was frozen. The ether phase was then washed with three successive 10 ml portions of the 10 M NH_4NO_3, 0.1 M HNO_3 solution.

16

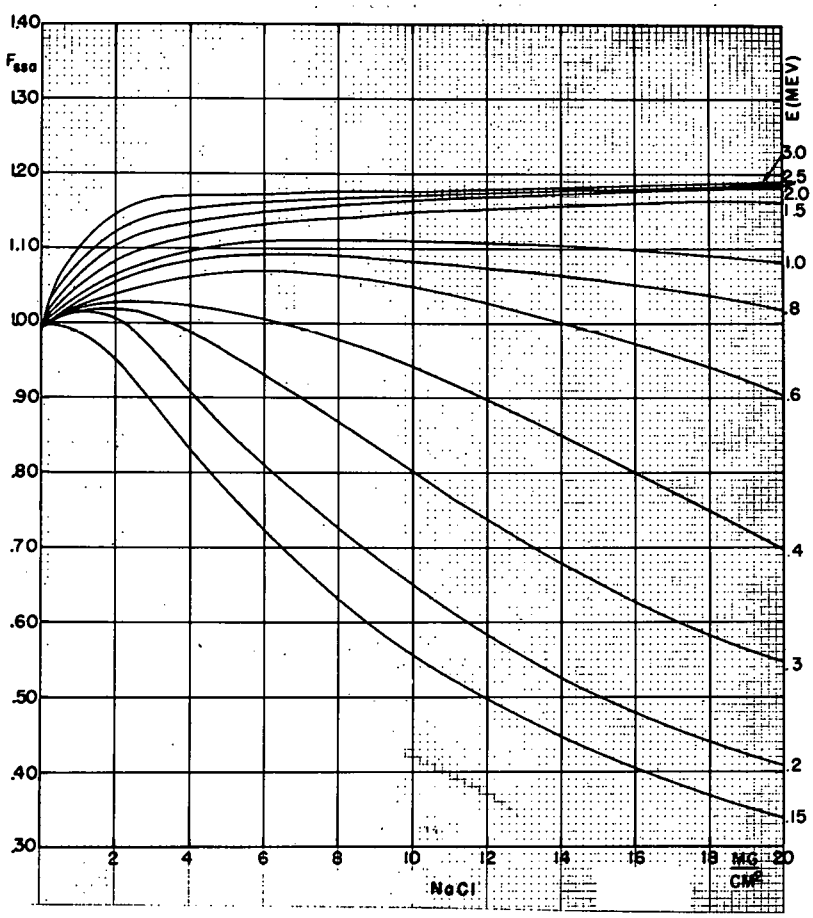

Fig. 4 — The correction factor, F_{SSA}, as a function of thickness of NaCl samples for convenient beta energies.

17

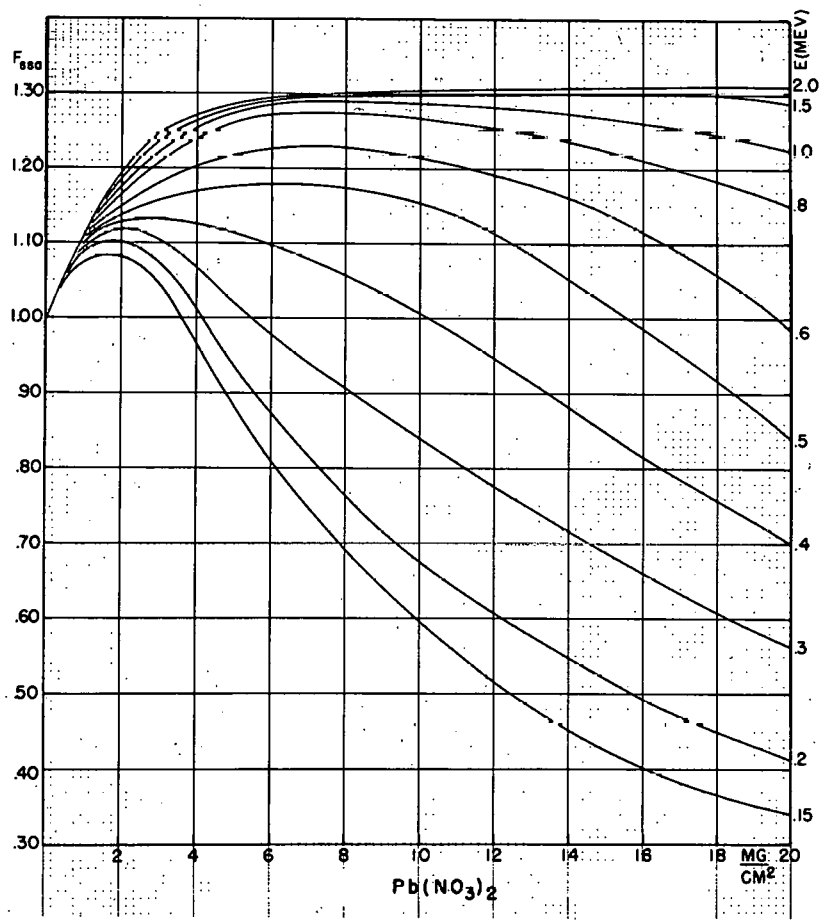

Fig. 5 — The correction factor, F_{SSA}, as a function of thickness of $Pb(NO_3)_2$ samples for convenient beta energies.

18

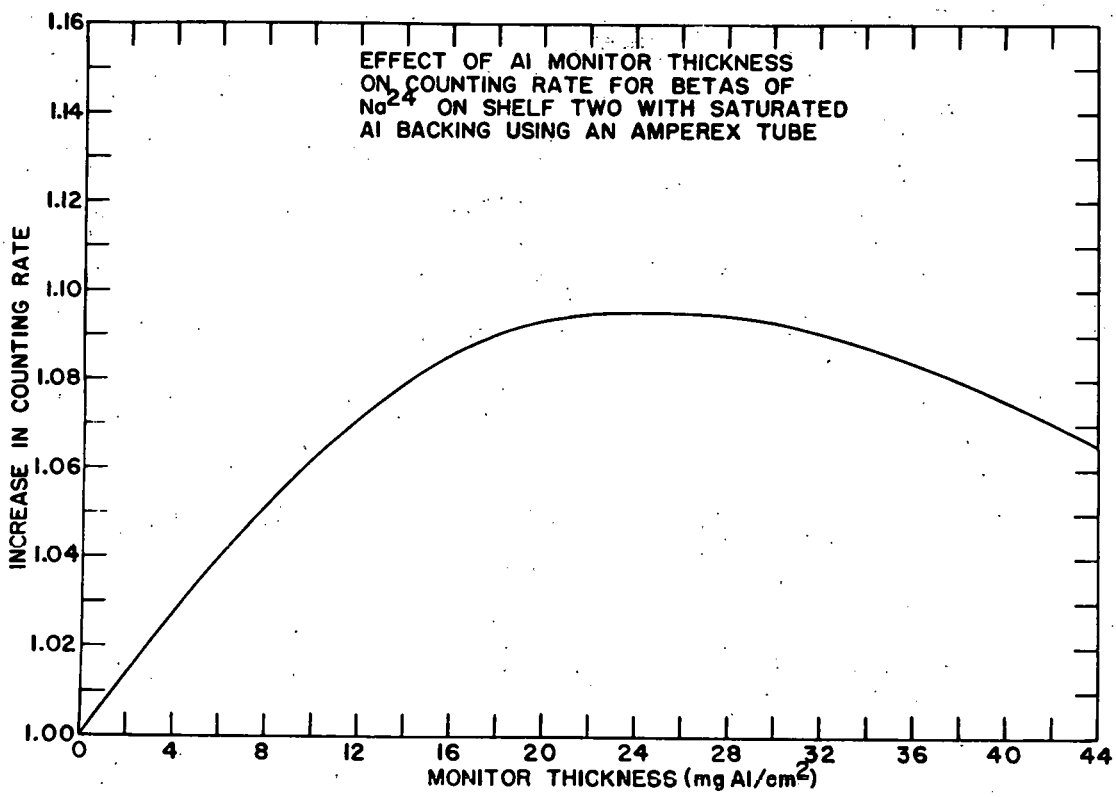

Fig. 6 — The effect of aluminum monitor thickness on the counting rate for the beta particles of Na^{24} on shelf two with saturated aluminum backing using an Amperex tube.

Uranium was backextracted from the ether by shaking with 15 ml of 0.1 M HNO_3 which was subsequently frozen and the ether discarded. Uranium hydroxide was precipitated with concentrated NH_4OH and centrifuged. The aqueous fraction was discarded and the uranium hydroxide was dissolved with concentrated HCl. The uranium was further purified by column techniques. Concentrated NH_4OH was added to the resulting solution and the precipitated uranium hydroxide was centrifuged and then washed with water and recentrifuged. The precipitate of uranium hydroxide was made into a thick slurry and part of it was transferred to a pre-weighed platinum "hat" with a transfer pipet. The slurry was dried with the aid of a heat lamp and then the platinum "hat" was strongly but carefully ignited in the flame of a Meeker burner to transform the uranium hydroxide to U_3O_8 and drive off any NH_4Cl. After cooling the platinum "hat" was weighed to determine the yield of uranium.

2. $Th^{232}(d,p)Th^{233}$ and $Th^{232}(d,n)Pa^{233}$.--The thorium target was dissolved in a small amount of concentrated HCl to which had been added a couple of drops of 1/5 M $(NH_4)_2SiF_6$. About 20 ml of concentrated HCl was added. If only the $Th^{232}(d,p)Th^{233}$ cross section was to be determined, initially formed protactinium was removed by column techniques. Pa^{231} tracer was then added to the thorium solution. The Pa^{231} tracer had been freshly extracted to ensure against colloidal protactinium. Three standard aliquots were taken and mounted on platinum plates. If the combined yield of the $Th^{232}(d,p)Th^{233}$ and $Th^{232}(d,n)Pa^{233}$ reactions was desired, Pa^{231} tracer was added to the

thorium solution and protactinium was not removed by column techniques. In both cases, after decay of the remaining Th^{233}, the thorium solution was made 8 M in HCl and extracted with two half-volumes of di-isopropyl ketone (DIPK) by shaking in a separatory funnel for a couple of minutes. The combined DIPK fractions were washed with two half-volumes of 8 M HCl. Protactinium was extracted from the DIPK with two half-volumes of 0.1 M HNO_3. The combined 0.1 M HNO_3 fractions were made 8 M in HCl and extracted four times with quarter-volumes of 0.4 M thenoyltrifluoroacetone (TTA) in benzene. The combined benzene fractions were reduced in volume with the aid of a heat lamp until essentially only TTA was left. A platinum plate was formed in the shape of an inverted cone and placed inside the coil of a 300 watt induction heater. The TTA was heated until liquefied and then transferred drop by drop to the center of the heated platinum plate with a transfer pipet. After every few drops the temperature of the platinum plate was carefully increased until all of the TTA had evaporated. After the last of the TTA had been evaporated the platinum plate was flattened into a disc again while still hot and then ignited in the flame of a Meeker burner. The yield of protactinium was determined by counting the alpha particles of Pa^{231} in the weightless sample and comparing the activity of the sample with the alpha activity of the three standard plates.

3. $Pt^{198}(d,p)Pt^{199}$.--The platinum target strip was cut into about a dozen small pieces. These were added to a No. 1 porcelain crucible approximately one-third filled with molten zinc and heated by a Meeker burner. The mixture was stirred for a few minutes with a glass rod to dissolve the platinum. The molten zinc was poured into a 600 ml

beaker containing about 1/2 inch of water. After cooling somewhat, the crucible with the remaining zinc stuck to it was added and concentrated HCl was added cautiously until hydrogen was no longer evolved. A finely divided black alloy of zinc and platinum resulted, from which it was easy to decant the supernatant liquid. The precipitate was washed with distilled water and again decanted. The alloy was quickly dissolved with a small amount of aqua regia. The solution was made 8 M in HCl and gold carrier added. The solution was extracted three times with equal volumes of ethyl acetate to remove all carrier and initially formed gold. Twenty milligrams of carrier gold was added at once to prevent loss of radioactive gold by exchange of gold ions for sodium ions on the surface of the glass. All the remaining Pt^{199} was allowed to decay and the gold was extracted with ethyl acetate until no further gold passed into the solvent as shown by its color. The ethyl acetate fraction was washed once with a half-volume of 8 M HCl and was then poured onto about 20 ml of 2 M HNO_3 in a beaker and was heated until all the ethyl acetate had evaporated. The resulting solution was made basic with ammonium hydroxide, heated, and a few ml of a concentrated solution of ascorbic acid was added. The resulting gold precipitate was digested for a short while in a water bath and centrifuged. The precipitate was washed with distilled water and again centrifuged. The gold was dissolved in a small amount of aqua regia and made 8 M in HCl. The extraction and precipitation cycle described above was repeated. The final gold precipitate was dissolved in the smallest possible amount of aqua regia. About 10 ml of a solution containing 2.5 g KCN per 100 ml distilled water was added.

The gold was deposited electrolytically on a pre-weighed one-inch diameter platinum plate cathode. Only an area 3/4-inch in diameter was exposed to the plating solution. The platinum plate was secured at the bottom of a small polystyrene tube immersed in water kept at a temperature of 55° C. A rotating anode, made out of a 1/8 inch diameter 10 percent iridium-platinum rod, was employed. The plating solution was electrolyzed until colorless using a current density of 0.024 amp/in^2. The resulting gold-plated platinum disc was washed first with distilled water, then ethyl alcohol, and finally diethyl ether and then dried in an oven at 110° C for 10 minutes. The yield of gold was determined by weighing.

4. $\underline{Pd^{110}(d,p)Pd^{111m} + Pd^{111g}}$.--The palladium target strip was dissolved in a few ml of aqua regia and the solution was diluted to 30 ml in a 40 ml centrifuge cone. In the first series of runs on the Berkeley 184-inch cyclotron the solution was allowed to stand until all Pd^{111g} had decayed to Ag^{111}. Twenty milligrams of silver carrier was then added to scavenge for all silver present. The resulting AgCl precipitate was centrifuged and discarded after being washed and the wash liquid added to the palladium solution. The scavenge was repeated with 20 mg more of silver. Twenty milligrams of silver carrier was added at once and the palladium solution was allowed to stand until all Pd^{111m} had decayed to Ag^{111}. It was important to add the carrier immediately after scavenging because silver ions like those of gold, but to a much greater extent, exchange with the sodium ions on the surface of the glass container. In the second series of

runs two silver scavenges were made as soon as possible and then silver carrier was added. The palladium solution was allowed to stand until essentially all of the Pd^{111g} had decayed. The solution was then centrifuged, the AgCl precipitate washed and retained. The wash liquid was added to the palladium solution and silver carrier was added and the solution allowed to stand until all the Pd^{111m} had decayed. In both cases the final AgCl precipitate was centrifuged, washed, and retained.

The AgCl was dissolved with a few ml of concentrated NH_4OH and the solution diluted to 20 ml. Twenty milligrams of Fe(+III) carrier was added and the resulting ferric hydroxide or hydrated iron oxide was centrifuged and discarded.

Hydrogen sulfide was bubbled in and the resulting Ag_2S centrifuged and washed. A few ml of concentrated HNO_3 was added and the mixture was heated to destroy the Ag_2S. The resulting solution was diluted to 20 ml in a 40 ml centrifuge cone and 20 mg of Fe(+III) carrier added. The ferric hydroxide precipitate was centrifuged and discarded. A couple of ml of concentrated HCl was added and the resulting AgCl was centrifuged and washed. The AgCl was dissolved in a few ml of concentrated NH_4OH and diluted to 20 ml. The solution was heated and a few ml of a concentrated solution of ascorbic acid was added. The resulting silver precipitate was digested for a short while in a water bath, centrifuged, and washed. The metallic silver was dissolved with a small amount of concentrated HNO_3 and the solution diluted to 20 ml. Twenty milligrams of Fe(+III) carrier was added and the solution made basic with concentrated NH_4OH. The

resulting ferric hydroxide was centrifuged and discarded. Hydrogen sulfide was again bubbled in and the above procedure was repeated to the point of dissolving the metallic silver in a small amount of concentrated HNO_3 and diluting to 20 ml with distilled water. Silver chloride was precipitated with a couple of ml of concentrated HCl. The precipitate was centrifuged and washed. The AgCl was dissolved in 8 ml of a solution containing 45 g KCN and 90 g K_2CO_3 per liter. The silver was electrodeposited on a platinum plate using the same arrangement as was used for gold deposition described above except that the anode was not rotated and the plating was done at room temperature. Also, the total current strength used was 0.01 amp, and the duration of the plating process was somewhat over one hour. The resulting silver deposit was washed with distilled water, ethyl alcohol, and diethyl ether. The plate was dried for 10 minutes at 110° C and weighed to determine the yield of silver.

5. $\underline{Zr^{96}(d,p)Zr^{97}}$.--The zirconium target strip was dissolved in 10 ml concentrated HCl to which had been added several drops of concentrated HF. The solution was chilled in an ice bath and saturated with HCl gas. Two milliliters of distilled water was added and the resulting solution was saturated with oxalic acid. The solution was scavenged for initially formed niobium by stirring with 15 ml DIPK in a 40 ml centrifuge cone for a couple of minutes. The resulting mixture was centrifuged and the DIPK phase removed with a transfer pipet and discarded. It was necessary to scavenge for niobium as many as ten or twelve times in this manner. However,

no zirconium was lost by this method. Ten milligrams of niobium carrier was added. It was in the form of Nb_2O_5 dissolved in 3 M NaOH. The solution was allowed to stand for about 3 hours and then it was again saturated with HCl gas in an ice bath. Two milliliters of water for every 10 ml of solution was added and the solution was saturated with oxalic acid. Niobium was extracted once with a double volume of DIPK. The DIPK phase was washed 3 times with 5 ml of a solution saturated with oxalic acid and of the same HCl concentration as the zirconium solution. Niobium was backextracted from the DIPK with two 10 ml portions of 6 M HCl. These were combined in a 100 ml Kjeldahl flask and 2 drops of phenolpthalein indicator added. The flask was chilled in a dry ice-acetone mixture and concentrated NH_4OH added very cautiously and slowly until the phenolpthalein endpoint was reached. The solution was kept chilled to prevent the resulting hydrated niobium oxide precipitate from going into the colloidal state. The precipitate was centrifuged and washed. About 7 ml of concentrated HNO_3 was added and the mixture heated. The mixture was diluted to 20 ml with distilled water and centrifuged. Twenty milliliters of water was added to the precipitate. Two drops of phenolpthalein indicator was added and the solution was brought to the phenolpthalein endpoint with concentrated NH_4OH. The precipitate was centrifuged and washed first with 40 ml absolute ethyl alcohol and then with 40 ml diethyl ether. The precipitate was left in the centrifuge cone and dried in a water bath. It was then transferred to a Vycor crucible and heated strongly in the flame of a Meeker burner for 10 minutes.

It was necessary to heat the precipitate at such a temperature that it assumed a yellow color. The resulting Nb_2O_5 was cooled and carefully powdered with a glass rod. The Nb_2O_5 powder was poured into a pre-weighed platinum "hat." The powder was evenly distributed and the platinum "hat" was heated strongly in the flame of a Meeker burner for a short while. After cooling, the platinum "hat" was weighed to determine the yield of niobium.

6. $\underline{Mn^{55}(d,p)Mn^{56}}$.--The manganese target was dissolved in several ml of 6 M HNO_3. Twenty milligrams of iron, five milligrams of scandium, and ten milligrams each of calcium, titanium, vanadium, and chromium carriers were added. The solution was diluted to 20 ml with distilled water and made basic with concentrated NH_4OH. The resulting precipitate was centrifuged and discarded. The solution was then made 10 M in HNO_3 and heated to the boiling point. Sufficient solid $KBrO_3$ was added slowly and cautiously to precipitate all the manganese as MnO_2. The precipitate was digested for a short while, centrifuged, and washed. The MnO_2 precipitate was dissolved with a small amount of concentrated HCl and diluted to approximately 30 ml. The solution was made strongly ammoniacal and just sufficient $(NH_4)_2S_2O_8$ was added to precipitate all the manganese as MnO_2. The solution was boiled in a hot water bath to cause precipitation of MnO_2 and to destroy any excess persulfate. The precipitate was centrifuged and washed several times with boiling water. The MnO_2 precipitate was dissolved with a couple of ml of concentrated HNO_3 and a few drops of 30 percent H_2O_2 and heated to destroy excess H_2O_2. Again the

same carriers were added as above, the solution was diluted to 20 ml and made basic with NH_4OH. The resulting precipitate was centrifuged and discarded. The solution was made 10 M in HNO_3 and heated to the boiling point. The cycle of two precipitations of MnO_2 with $KBrO_3$ and $(NH_4)_2S_2O_8$ was repeated twice more except that before the last complete cycle only 20 mg of iron carrier was added. After the MnO_2 precipitate from the final persulfate precipitation was dissolved, 20 mg of iron carrier was added, the solution was diluted to 20 ml and made basic with NH_4OH. The resulting precipitate was centrifuged and discarded and the solution was made 10 M in HNO_3. The solution was heated to the boiling point, and MnO_2 was precipitated with $KBrO_3$ as above. The precipitate was centrifuged and washed very well. A slurry was made of the precipitate and part of it was placed in a pre-weighed platinum "hat" with the aid of a transfer pipet. The precipitate was cautiously partially dried with a heat lamp. Too great heat would decompose the MnO_2. Because of the voluminous nature of the precipitate and consequent shrinkage upon drying, additions of the slurry were made to the platinum "hat." When enough sample had been accumulated, the drying of the sample was accomplished in an oven at 110° C. After cooling, the platinum "hat" was weighed to ascertain the yield of manganese.

D. RESULTS

1. $U^{238}(d,p)U^{239}$.--The 23.54 minute half-life activity of U^{239} was counted directly. This was resolved from a relatively small tail composed of activities of considerably longer half-life.

Five separate runs were made on the Berkeley 60-inch cyclotron giving a total of 25 samples representing cross sections at energies from 5.98 to 19.82 Mev. Eight bombardments were made on the Berkeley 184-inch cyclotron ranging in energy from 50 to 174 Mev.

An aluminum wrapped piece of uranium was placed behind the copper lips of a "clothes-pin" type target holder (0.25-0.40 inch in thickness) about 7 mm away from the leading edge of an uranium target. The assembly was bombarded with full energy deuterons. The U^{239} activity induced in the shielded piece of uranium indicated that the contribution of the neutron background in the tank in forming U^{239} by the (n,γ) reaction amounted to at most probably a few percent of the total observed U^{239} cross sections. The effect of the (n,γ) reaction on cross sections for formation of the other nuclides studied was considered to be about the same or smaller.

In 60-inch bombardments on uranium and thorium, the activity induced in foils beyond where the deuteron energy has been degraded to zero indicated that, as an approximate limit, 2 percent of the total cross section at the peak of the excitation functions for the production of U^{239} and Th^{233} was caused by the (n,γ) reaction. The neutron background should be proportionately much higher for 60-inch than for 184-inch cyclotron runs due to the thicker targets used and the fact that the 1/8 inch collimated beam of deuterons reaching the target represents only about 5 percent of the total number of deuterons striking the aluminum collimator.

29

In Tables 1 through 5 may be found values of the cross section for the $U^{238}(d,p)U^{239}$ reaction for various deuteron energies as obtained from the five runs on the Berkeley 60-inch cyclotron. Selfscattering factors for the various sample thicknesses are also included in the tables. The same selfscattering factors for U_3O_8 as for $Pb(NO_3)_2$ are assumed. The air/window correction factor was taken as 1.069.

Table 1

$U^{238}(d,p)U^{239}$; run 1 on the Berkeley 60-inch cyclotron.

mg U^{238}/cm^2	Deuteron Energy (Mev)	$\sigma_{U^{239}}$ (mb)	mg U_3O_8/cm^2	f_{ss} U_3O_8
345.9	13.30	174	1.49	1.15
378.2	12.60	139	3.22	1.23
409.0	11.80	121	2.96	1.23
439.1	11.05	95.7	3.01	1.23

Table 2

$U^{238}(d,p)U^{239}$; run 2 on the Berkeley 60-inch cyclotron.

mg U^{238}/cm^2	Deuteron Energy (Mcv)	$\sigma_{U^{239}}$ (mb)	mg U_3O_8/cm^2	f_{ss} U_3O_8
160.0	19.80	113	7.78	1.29
178.6	19.05	127	6.40	1.29
183.1	18.30	130	6.75	1.29
176.8	17.50	125	8.65	1.29
194.1	16.75	138	6.34	1.29

30

Table 3

$U^{238}(d,p)U^{239}$; run 3 on the Berkeley 60-inch cyclotron.

mg U^{238}/cm^2	Deuteron Energy (Mev)	$\sigma_{U^{239}}$ (mb)	mg U_3O_8/cm^2	f_{ss} U_3O_8
267.4	15.10	170	7.54	1.29
311.2	14.15	176	5.70	1.28
356.0	13.10	174	6.70	1.29
399.3	12.05	151	5.15	1.28
439.2	11.05	125	5.36	1.28
476.4	10.00	84.7	5.94	1.28

Table 4

$U^{238}(d,p)U^{239}$; run 4 on the Berkeley 60-inch cyclotron.

mg U^{238}/cm^2	Deuteron Energy (Mev)	$\sigma_{U^{239}}$ (mb)	mg U_3O_8/cm^2	f_{ss} U_3O_8
125.0	17.95	133	6.94	1.29
172.6	17.05	143	8.21	1.29
219.3	16.10	166	7.90	1.29
265.1	15.10	165	6.54	1.29
311.0	14.15	173	9.21	1.30
356.8	13.10	166	7.86	1.29

Table 5

$U^{238}(d,p)U^{239}$; run 5 on the Berkeley 60-inch cyclotron.

mg U^{238}/cm^2	Deuteron Energy (Mev)	$\sigma_{U^{239}}$ (mb)	mg U_3O_8/cm^2	f_{ss} U_3O_8
476.2	10.05	101	54.7	0.98
522.2	8.70	57.9	36.1	1.13
565.2	7.35	29.7	64.5	0.90
608.1	6.00	7.5	39.4	1.10

Table 6 lists the results of the deuteron bombardments on uranium using the Berkeley 184-inch cyclotron.

Table 6

$U^{238}(d,p)U^{239}$; runs on the Berkeley 184-inch cyclotron.

Deuteron Energy (Mev)	$\sigma_{U^{239}}$ (mb)	mg U_3O_8/cm^2	f_{ss} U_3O_8	Avg. mg Al/cm^2	f_{ss} Al
50	17.4	4.21	1.26	3.44	1.024
60	14.9	8.60	1.30	3.58	1.025
75	10.3	5.67	1.28	3.43	1.024
85	8.1_1	8.86	1.30	3.58	1.025
100	6.1_9	6.30	1.29	3.44	1.024
125	3.9_9	11.92	1.29	3.51	1.025
150	2.9_5	10.67	1.30	3.51	1.025
174	2.6_8	2.48	1.20	3.44	1.024

The $U^{238}(d,p)U^{239}$ excitation function in the ranges of the Berkeley 60-inch and 184-inch cyclotrons is given in Figures 7 and 8;

32

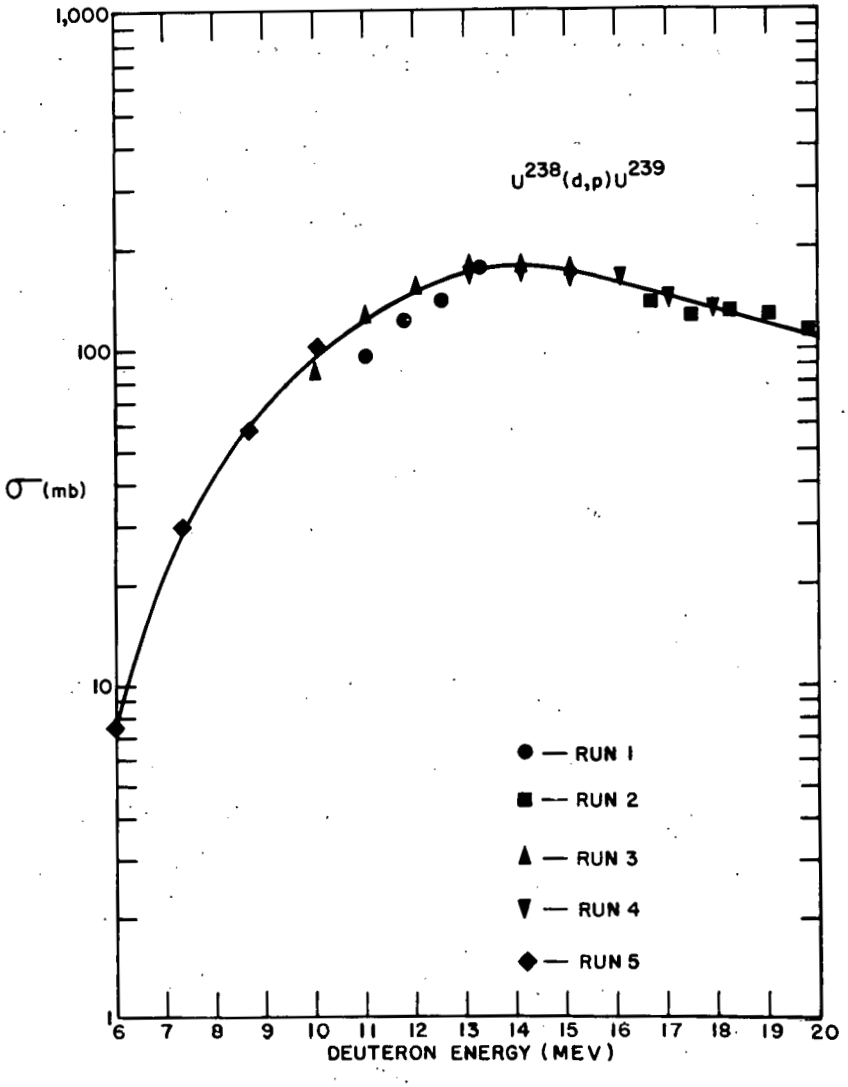

Fig. 7 — $U^{238}(d,p)U^{239}$ excitation function in the range of the Berkeley 60-inch cyclotron.

33

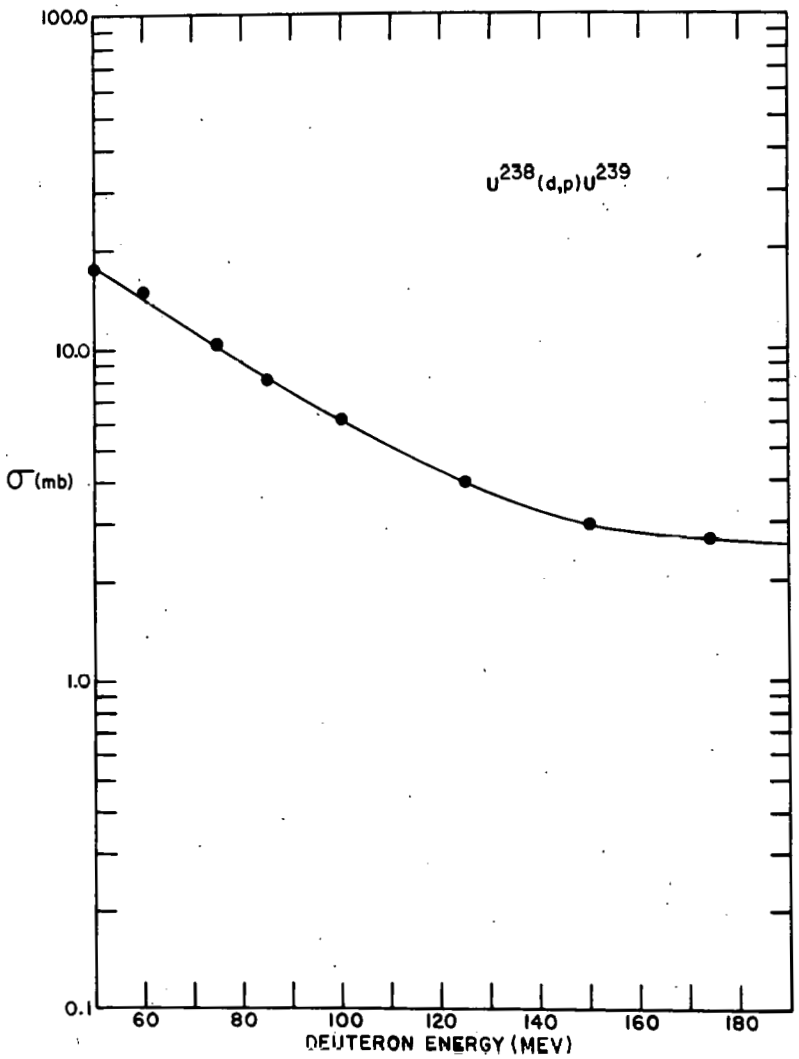

Fig. 8 — $U^{238}(d,p)U^{238}$ excitation function in the range of the Berkeley 184-inch cyclotron.

respectively. Both sections are shown together in Figure 11. The values of the cross sections given by this excitation function, as well as cross section values for all other excitation functions given later, should be accurate within ±20 percent for that portion of the excitation function down to the area of the peak. Beyond the relatively flat area of the curve near the peak, values of the cross section become increasingly unreliable. In a stacked foil experiment, especially with low energy particles, range straggling causes an energy spread, ΔE, amongst even originally monoenergetic deuterons that increases with increasing target thickness. In addition, an initial energy spread, ΔE_o, of the deuterons from the 60-inch cyclotron increases as E^{-1} with increasing target thickness. A third cause of energy spread is the accumulated nonuniformities in individual foil thicknesses. Thus part of the beam will probably see a somewhat thicker or thinner target than the rest.

2. $Th^{232}(d,p)Th^{233}$.--The yield of the 23.3 minute half-life Th^{233} was obtained from the activity of the daughter Pa^{233}. Correction was made for the decay of Th^{233} from the time of bombardment to the time of separation of all initially formed protactinium. The 27.4 day half-life Pa^{233} is the only activity seen in the finally separated protactinium fraction. Tables 7 through 9 list results of three runs on the Berkeley 60-inch cyclotron. Difficulties arose in measuring the beam current in the first and third runs. Shorts in the cirquit resulted in apparent total beam currents in excess of the actual. Because of this, the

cross sections obtained in these runs are given in the tables normalized to the highest and most correct of the three runs, number two.

Table 7

$Th^{232}(d,p)Th^{233}$; run 1 on the Berkeley 60-inch cyclotron.

mg Th^{232}/cm^2	Deuteron Energy (Mev)	σ (mb)
14.06	20.00	106
70.24	18.95	123
125.8	18.00	130
184.2	16.90	147
298.8	14.40	169
356.6	13.00	162
414.3	11.70	159
473.0	10.10	115
532.8	8.40	51.4
594.5	6.40	13.8
655.9	4.25	1.9
718.5	~2	4.7
780.7	~0	3.6

Table 8

$Th^{232}(d,p)Th^{233}$; run 2 on the Berkeley 60-inch cyclotron.

mg Th^{232}/cm^2	Deuteron Energy (Mev)	σ (mb)
13.93	20.00	117
42.44	19.45	120
71.88	18.95	119
101.1	18.40	124
130.3	17.85	128
159.4	17.30	138
188.3	16.70	151
217.3	16.20	147
246.2	15.55	154
275.0	14.90	167
303.7	14.30	164
332.8	13.65	163
361.9	12.95	169
391.5	12.25	163
451.1	10.70	107
481.3	9.90	76.2
511.1	9.00	66.8
540.6	8.10	24.2
569.8	7.20	8.8
599.2	6.25	3.9
629.1	5.20	2.6

37

Table 9

$Th^{232}(d,p)Th^{233}$; run 3 on the Berkeley 60-inch cyclotron.

mg Th^{232}/cm^2	Deuteron Energy (Mev)	σ (mb)
45.34	19.40	116
104.0	18.35	133
163.1	17.20	137
223.9	16.00	155
285.6	14.70	161
343.0	13.40	154
413.6	11.70	121
487.3	9.70	48.3
561.2	7.50	3.4
634.8	5.00	1.5

The values of the cross section for the $Th^{232}(d,p)Th^{233}$ excitation function become increasingly unreliable for deuteron energies below the area of the peak for the reasons given in connection with the $U^{238}(d,p)U^{239}$ reaction. However, in the case of thorium there is an additional complication. The initial counting rate of many of the samples was well below 50 counts/minute, some around 10 or lower. The resulting statistics and the possible presence of a very small amount of impurity hindered the drawing of a satisfactory decay line. The small initial counting rate was the result of small cross sections at low deuteron energies, small beam current passed by the collimator, and the relatively long

half-life of Pa^{233} compared with U^{239}, as well as poor chemical yield in some cases. Long bombardments were ruled out because of the 23.3 minute half-life of Th^{233}. As has been pointed out earlier, the effect of neutron background is small for observed cross sections near the peak in deuteron bombardments on the Berkeley 60-inch cyclotron. However, the contribution of the (n,γ) reaction becomes relatively of increasing importance for small deuteron energies where the (d,p) cross section values are small. No corrections for this effect have been made in the given excitation functions on uranium or thorium. There are two reasons for this. First, the neutron background is not a constant for all of the stacked foils but should increase with increasing target thickness. Secondly, the same correction cannot be made, per given number of deuterons striking the target, from one bombardment to another since the percentage of deuterons passed by the collimator of the total number striking it usually varies.

The results of the deuteron bombardments on thorium using the Berkeley 184-inch cyclotron are given in Table 10.

Table 10

$Th^{232}(d,p)Th^{233}$; runs on the Berkeley 184-inch cyclotron.

Deuteron Energy (Mev)	σ (mb)	mg Al/cm^2	$f_{ss\ Al}$
50	23.2_2	7.68	1.050
100	5.4_1	7.64	1.050
150	2.9_3	7.68	1.050
190	1.9_3	7.64	1.050

39

Figures 9 and 10 give graphically the $Th^{232}(d,p)Th^{233}$ excitation function in the ranges of the Berkeley 60-inch cyclotron and the Berkeley 184-inch cyclotron, respectively. Both sections are shown together in Figure 11.

3. $Th^{232}(d,n)Pa^{233}$.--In the first Berkeley 60-inch cyclotron deuteron bombardment on thorium, alternate thorium foils were worked up without removal of initially formed protactinium. In the energy range encountered, only Pa^{233} was detectable in the resulting protactinium fraction. This represented the combined yields of the $Th^{232}(d,p)Th^{233}$ and $Th^{232}(d,n)Pa^{233}$ reactions as all of the Th^{233} had decayed to Pa^{233} before the foils were worked up. Table 11 gives the observed combined cross section for the two reactions.

Table 11

$Th^{232}(d,p)Th^{233}$ plus $Th^{232}(d,n)Pa^{233}$; run 1 on the Berkeley 60-inch cyclotron.

mg Th^{232}/cm^2	Deuteron Energy (Mev)	σ (mb)
42.86	19.50	125
96.82	18.50	153
155.0	17.50	166
213.6	16.25	202
270.4	15.05	199
327.7	13.80	216
385.6	12.40	202
443.3	10.90	175
502.6	9.30	103
563.4	7.50	29.4
625.5	5.35	17.8
686.8	3.10	10.2
749.5	~1	1.7

40

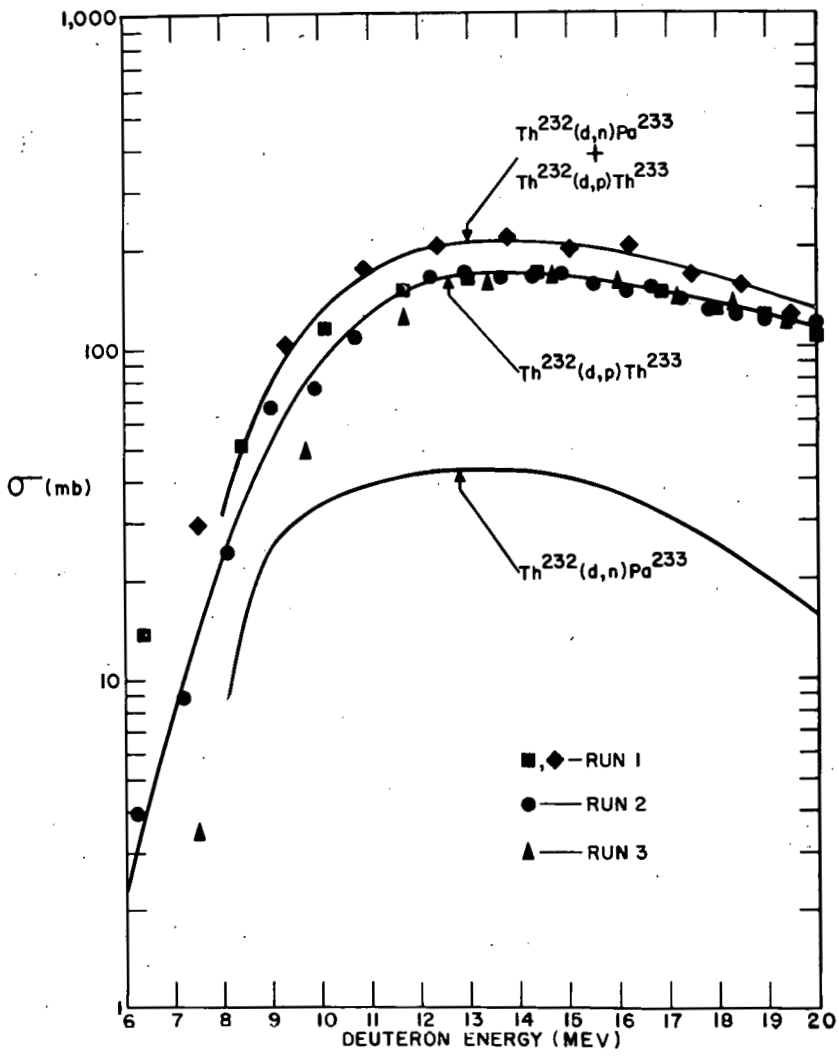

Fig. 9 — $Th^{232}(d,p)Th^{233}$ and $Th^{232}(d,n)Pa^{233}$ excitation functions in the range of the Berkeley 60-inch cyclotron.

41

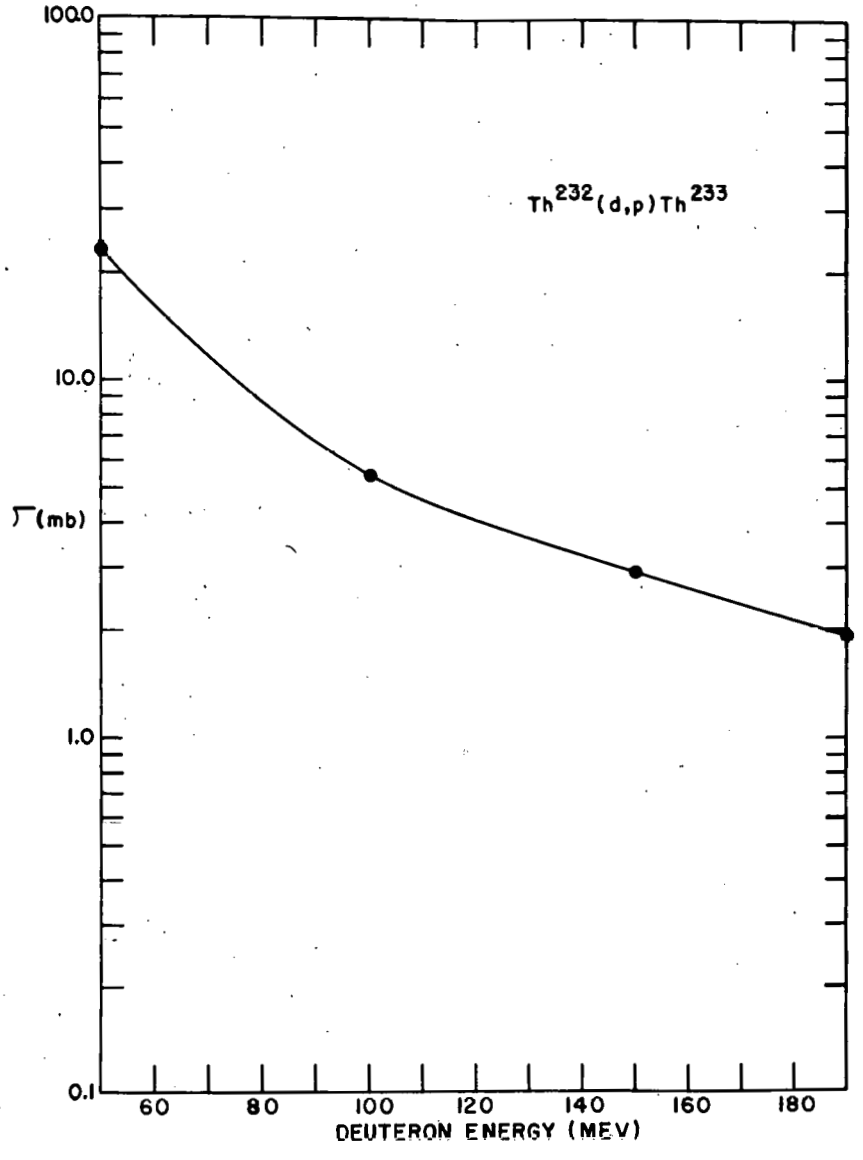

Fig. 10 — $Th^{232}(d,p)Th^{233}$ excitation function in the range of the Berkeley 184-inch cyclotron.

42

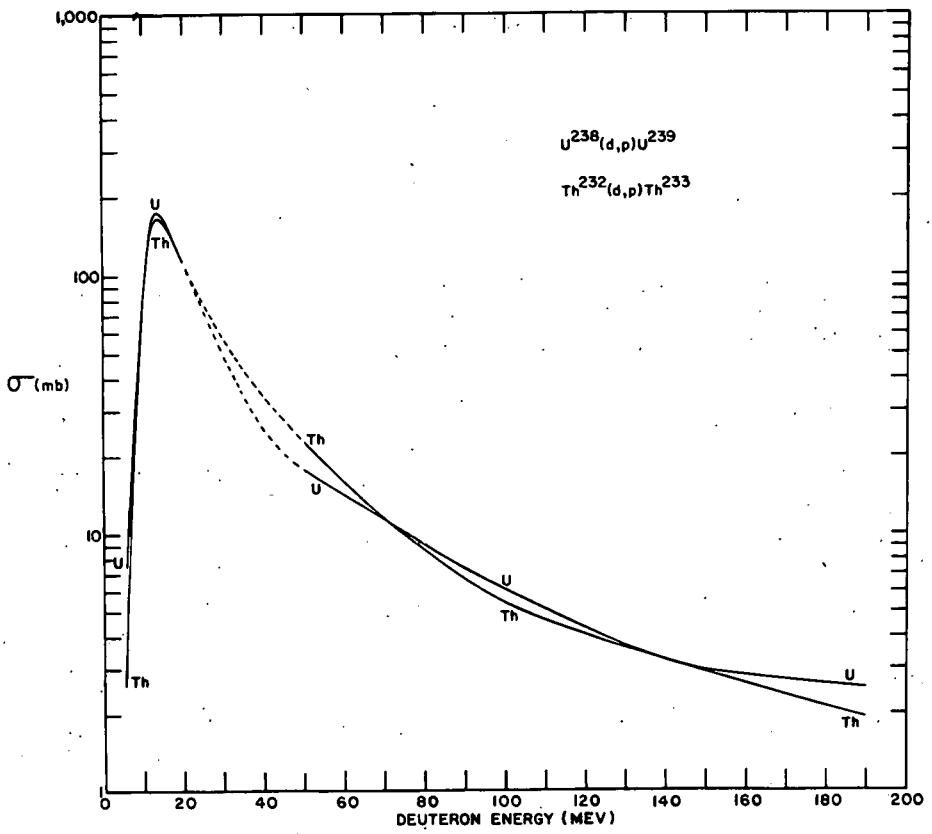

Fig. 11 — Comparison of the $U^{238}(d,p)U^{239}$ and the $Th^{232}(d,p)Th^{233}$ excitation functions.

Figure 9 gives the combined excitation function as well as the $Th^{232}(d,n)Pa^{233}$ excitation function as obtained from the difference of the combined and the $Th^{232}(d,p)Th^{233}$ excitation functions. Values of the cross section of the $Th^{232}(d,n)Pa^{233}$ excitation function are quite unreliable for deuteron energies below the area of the peak due to the fact that they are obtained from the difference of two relatively large figures, both subject to rather large errors.

4. $Pt^{198}(d,p)Pt^{199}$.--Cross sections for the formation of Pt^{199} were obtained from the activity of the daughter, 3.15 day half-life Au^{199}, in the final gold fraction. Au^{199} was the only activity in this fraction. Correction was made for the decay of 31 minute half-life Pt^{199} from the time of bombardment to the time of removal of initially formed gold. The combined air-window correction factor for the three beta particles of Au^{199} is 1.760; the combined saturated platinum backscattering factor is 1.560. Combined selfscattering corrections were obtained by assuming the same factors for gold as for $Pb(NO_3)_2$. Table 12 gives the results of deuteron bombardments on platinum using the Berkeley 184-inch cyclotron. These results are shown graphically in Figure 12.

Table 12

$Pt^{198}(d,p)Pt^{199}$; runs on the Berkeley 184-inch cyclotron.

Deuteron Energy (Mev)	σ (mb)	mg Au/cm^2	$f_{ss\ Au}$	Avg. mg Al/cm^2	$f_{ss\ Al}$
50	29.7	6.34	0.959	6.31	1.042
100	10.7	5.80	0.980	6.33	1.042
150	3.5_2	6.40	0.958	6.27	1.042
190	1.9_7	6.07	0.969	6.31	1.042

44

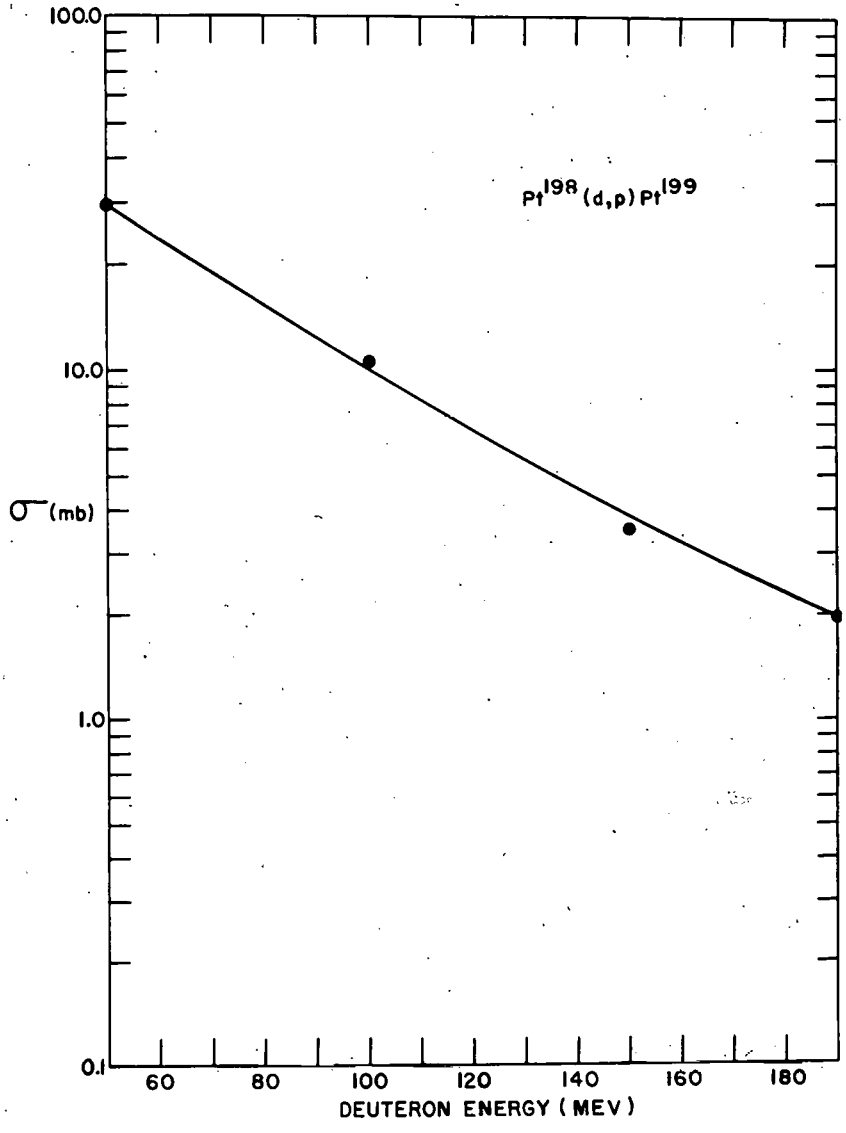

Fig. 12 — $Pt^{198}(d,p)Pt^{199}$ excitation function in the range of the Berkeley 184-inch cyclotron.

5. $\underline{Pd^{110}(d,p)Pd^{111g} + Pd^{111m}}$.--Two series of deuteron bombardments on palladium were completed using the Berkeley 184-inch cyclotron. In the first series all of the 22 minute half-life Pd^{111g} was allowed to decay before the samples were scavenged to remove all silver. Thus only the yield of the 5.5 hour half-life isomer Pd^{111m} was measured. This was obtained from the activity of the daughter, 7.6 day half-life Ag^{111}, in the silver fraction removed after decay of all Pd^{111m}. The only observable activity in that fraction was due to Ag^{111}. The number of originally formed atoms of Pd^{111m}, taking into account its 75 percent decay to Pd^{111g}, can be calculated from the number of remaining atoms of Ag^{111} at any time, t, after the time of silver scavenge as follows:

$$N^{t}_{Ag^{111}} = \frac{e^{-\lambda_{Ag^{111}} t} \times e^{-\lambda_{Pd^{111m}} T} \times 0.25 \times C \times \lambda_{Pd^{111m}} \times N^{o}_{Pd^{111m}}}{(\lambda_{Pd^{111m}} - \lambda_{Ag^{111}})} \times \left[1 + \frac{3\lambda_{Pd^{111g}}}{(\lambda_{Pd^{111g}} - \lambda_{Pd^{111m}})}\right]$$

T is the length of time from the end of bombardment to the time of silver scavenge. C is the correction factor used here and in all other cases to correct for length of bombardment comparable to the half-life of the product nuclide and is calculated as follows:

$$C = \frac{(1 - e^{-\lambda_{Pd^{111m}} t})}{\lambda_{Pd^{111m}} t}$$

t here is the length of bombardment.

In the second series of bombardments, all initially produced silver was removed as soon as possible. After this, silver was milked from the sample twice; once when most of the Pd^{111g} and some of the Pd^{111m} had decayed, and secondly when all the rest of the Pd^{111g} and Pd^{111m} had decayed. Let $N^{t}_{Ag^{111}}$ - II be the number of atoms of Ag^{111} resulting from the first milking remaining at the same time or t + T after the initial silver scavenge. T is the length of time between the time of scavenge and that of the first milking. Allowing τ to be the time from the end of bombardment to the time of scavenge we obtain the following relations:

$$N^{t}_{Ag^{111}} - II = e^{-\lambda_{Ag^{111}} t} \left[\frac{0.25\, C_2\, N^{o}_{Pd^{111m}}\, \lambda_{Pd^{111m}}\, e^{-\lambda_{Pd^{111m}} (T + \tau)}}{(\lambda_{Pd^{111m}} - \lambda_{Ag^{111}})} \right.$$

$$\left. + \frac{C_1 \lambda_{Pd^{111g}}\, N^{o}_{Pd^{111g}}\, e^{-\lambda_{Pd^{111g}} (T + \tau)}}{(\lambda_{Pd^{111g}} - \lambda_{Ag^{111}})} \right]$$

$$+ \left[\frac{0.75\, C_2 \lambda_{Pd^{111g}} \lambda_{Pd^{111m}}\, N^{o}_{Pd^{111m}}\, e^{-\lambda_{Ag^{111}} t}}{(\lambda_{Pd^{111g}} - \lambda_{Pd^{111m}})} \right]$$

$$\times \left[\frac{e^{-\lambda_{Pd^{111m}} (T + \tau)}}{(\lambda_{Pd^{111m}} - \lambda_{Ag^{111}})} - \frac{e^{-\lambda_{Pd^{111g}} (T + \tau)}}{(\lambda_{Pd^{111g}} - \lambda_{Ag^{111}})} \right].$$

$$N^{t+T}_{Ag111} = - \frac{0.25\, C_2 N^{o}_{Pd111m}\, \lambda_{Pd111m}\, e^{-\lambda_{Pd111m}\tau}\, e^{-\lambda_{Ag111}\, t}}{(\lambda_{Pd111m} - \lambda_{Ag111})}$$

$$\times \left(e^{-\lambda_{Pd111m}\, T} - e^{-\lambda_{Ag111}\, T}\right)$$

$$- \frac{C_1 \lambda_{Pd111g}\, N^{o}_{Pd111g}\, e^{-\lambda_{Pd111g}\tau}\, e^{-\lambda_{Ag111}\, t}}{(\lambda_{Pd111g} - \lambda_{Ag111})} \times \left(e^{-\lambda_{Pd111g}\, T} - e^{-\lambda_{Ag111}\, T}\right)$$

$$+ \frac{0.75\, C_2 \lambda_{Pd111g}\, \lambda_{Pd111m}\, N^{o}_{Pd111m}\, e^{-\lambda_{Ag111}\,(t+T)}}{(\lambda_{Pd111g} - \lambda_{Pd111m})}$$

$$\times \left[\frac{e^{-\lambda_{Pd111m}\tau}}{(\lambda_{Pd111m} - \lambda_{Ag111})} - \frac{e^{-\lambda_{Pd111g}\tau}}{(\lambda_{Pd111g} - \lambda_{Ag111})}\right]$$

$$- \frac{0.75\, C_2 \lambda_{Pd111g}\, \lambda_{Pd111m}\, N^{o}_{Pd111m}\, e^{-\lambda_{Ag111}\, t}}{(\lambda_{Pd111g} - \lambda_{Pd111m})}$$

$$\times \left[\frac{e^{-\lambda_{Pd111m}\,(\tau+T)}}{(\lambda_{Pd111m} - \lambda_{Ag111})} - \frac{e^{-\lambda_{Pd111g}\,(\tau+T)}}{(\lambda_{Pd111g} - \lambda_{Ag111})}\right] .$$

C_1 and C_2 are the correction factors for the length of bombardment comparable to the half-lives of Pd^{111g} and Pd^{111m}, respectively. Initial yields of both isomers can be calculated from the Ag^{111} activity in both milkings by means of the relations given above.

The results of the two series of bombardments are given in Tables 13, 14, and 15 and are shown graphically in Figure 13. In Table 15 is given the ratio of the cross section of formation of Pd^{111m} to that of Pd^{111g} at various deuteron energies in the second series of runs. The composite air-window correction factor for the beta particles of Ag^{111} was taken as 1.087. The selfscattering factors for the three beta particles in silver were obtained from the average of the factors for the beta particles in $Pb(NO_3)_2$ and NaCl.

Table 13

$Pd^{110}(d,p)Pd^{111m}$; first series of runs on the Berkeley 184-inch cyclotron.

Deuteron Energy (Mev)	σ (mb)	mg Ag/cm^2	$f_{ss\ Ag}$	Avg. mg Al/cm^2	$f_{ss\ Al}$
50	4.7_3	1.24	1.090	3.48	1.024
100	2.3_4	2.16	1.129	3.48	1.024
150	0.69	2.70	1.144	3.51	1.024
190	0.29	2.36	1.132	3.51	1.024

Table 14

$Pd^{110}(d,p)Pd^{111m}$; second series of runs on the Berkeley 184-inch cyclotron.

Deuteron Energy (Mev)	σ (mb)	mg Ag/cm^2	$f_{ss\ Ag}$	Avg. mg Al/cm^2	$f_{ss\ Al}$
50	4.85	4.49	1.182	3.55	1.025
100	2.40	4.61	1.184	3.55	1.025
150	0.76	2.35	1.132	3.51	1.025
190	0.36	2.30	1.130	3.51	1.025

49

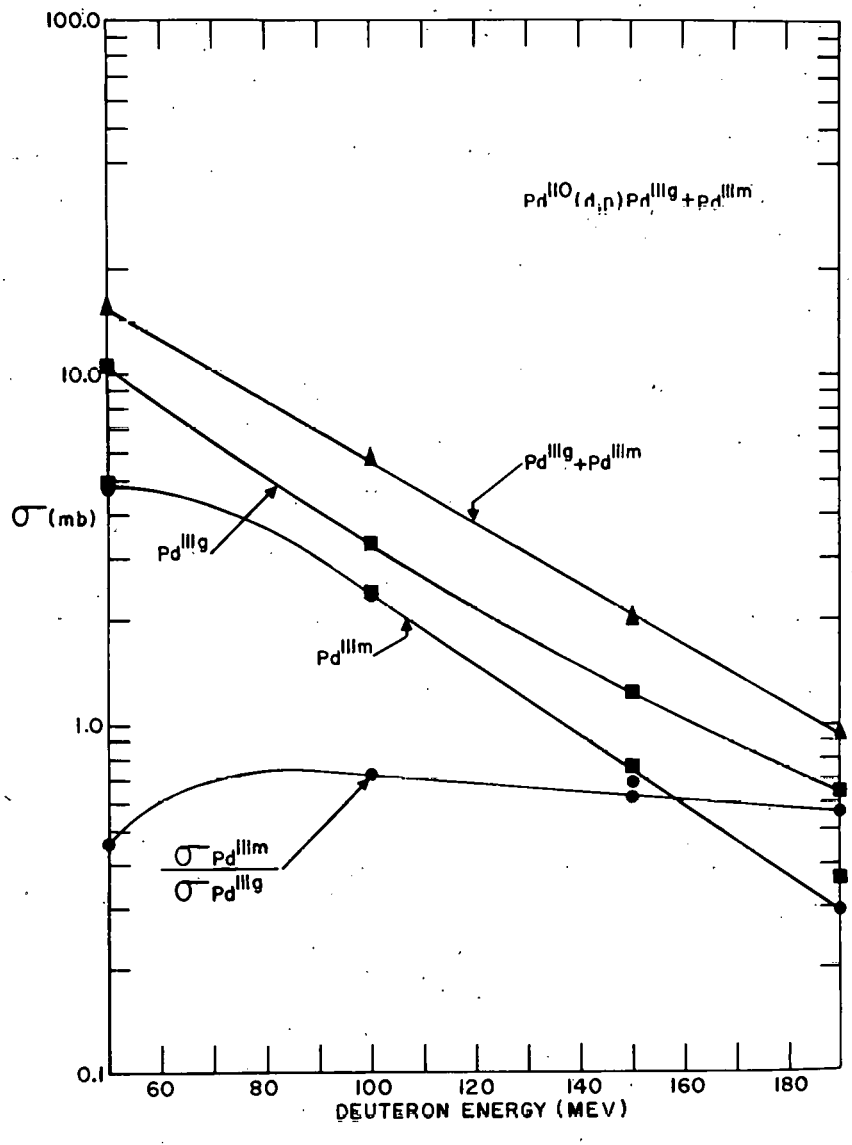

Fig. 13 — $Pd^{110}(d,p)Pd^{111m}$ and $Pd^{110}(d,p)Pd^{111g}$ excitation functions in the range of the Berkeley 184-inch cyclotron.

50

Table 15

$Pd^{110}(d,p)Pd^{111g}$; second series of runs on the Berkeley 184-inch cyclotron.

Deuteron Energy (Mev)	σ (mb)	$\frac{\sigma_{Pd^{111m}}}{\sigma_{Pd^{111g}}}$	mg Ag/cm^2	f_{ss} Ag	Avg. mg Al/cm^2	f_{ss} Al
50	10.6	0.460	2.60	1.140	3.55	1.025
100	3.30	0.728	2.50	1.138	3.55	1.025
150	1.23	0.618	1.60	1.104	3.51	1.025
190	0.64	0.564	1.57	1.101	3.51	1.025

It should be mentioned that C. L. McGinnis[7] reports that Pd^{111g} decays to an excited state of Ag^{111} whose 60 kev conversion electrons have been observed. On the basis of the shell model he makes the following assignments: Pd^{111m} - $h_{11/2}$, Pd^{111g} - $d_{5/2}$, Ag^{111m} - 7/2, and Ag^{111} - $p_{1/2}$. P. C. Stevenson and H. G. Hicks[4] report the existence of Ag^{111m} with a half-life of less than five minutes. Yield considerations of Ag^{111} from Pd^{111m} and Pd^{111g} indicate some β^- branching in Ag^{111m}. Ag^{111m} has been given an F classification. The existence of a short-lived β^- active isomer of Ag^{111} could result in errors in the cross section values given above.

6. $Zr^{96}(d,p)Zr^{97}$.--The yield of Zr^{97}, obtained in deuteron bombardments on Zr^{96} using the Berkeley 184-inch cyclotron, was measured by the activity of Nb^{97} that had grown into the niobium fraction taken from the zirconium sample after removal of

initially formed niobium. The 72.1 minute half-life Nb^{97} is the daughter of 60 second half-life Nb^{97m} to which 17 hour half-life Zr^{97} decays.

It was difficult to remove all of the initially formed niobium without causing loss of zirconium. The same separation of niobium from zirconium was used for both the scavenging and the milking. This separation allowed no weighable amounts of zirconium to be carried over with the niobium carrier. However, a tail resulted in the decay of activities in the final niobium fraction. The tail consisted largely of 15.0 hour half-life Nb^{90} activity with a small amount of longer-lived niobium activity. Very good 72.1 minute half-life lines of Nb^{97} activity were resolved by subtraction of the tail activity from the gross activity.

Let T_1 and T_2 represent respectively the times of bombardment and initially formed niobium scavenge. If t is allowed to represent the length of time from niobium scavenge to final niobium milking, the following relation allows the determination of the initial number of Zr^{97} atoms formed in the bombardment:

$$(N_{Zr^{97}})_{T_1} = \left(\frac{dN_{Nb^{97}}}{dt}\right)_t \left[\frac{(\lambda_{Nb^{97}} - \lambda_{Zr^{97}})}{\lambda_{Nb^{97}}\,\lambda_{Zr^{97}}\,(e^{-\lambda_{Zr^{97}}} - e^{-\lambda_{Nb^{97}}})}\right] e^{\lambda_{Zr^{97}}(T_2 - T_1)}$$

The results of the deuteron bombardments on zirconium using the Berkeley 184-inch cyclotron are listed in Table 16 and are shown graphically in Figure 14. The air-window correction factor used for the 1.267 Mev maximum energy beta particle of Nb^{97} is

52

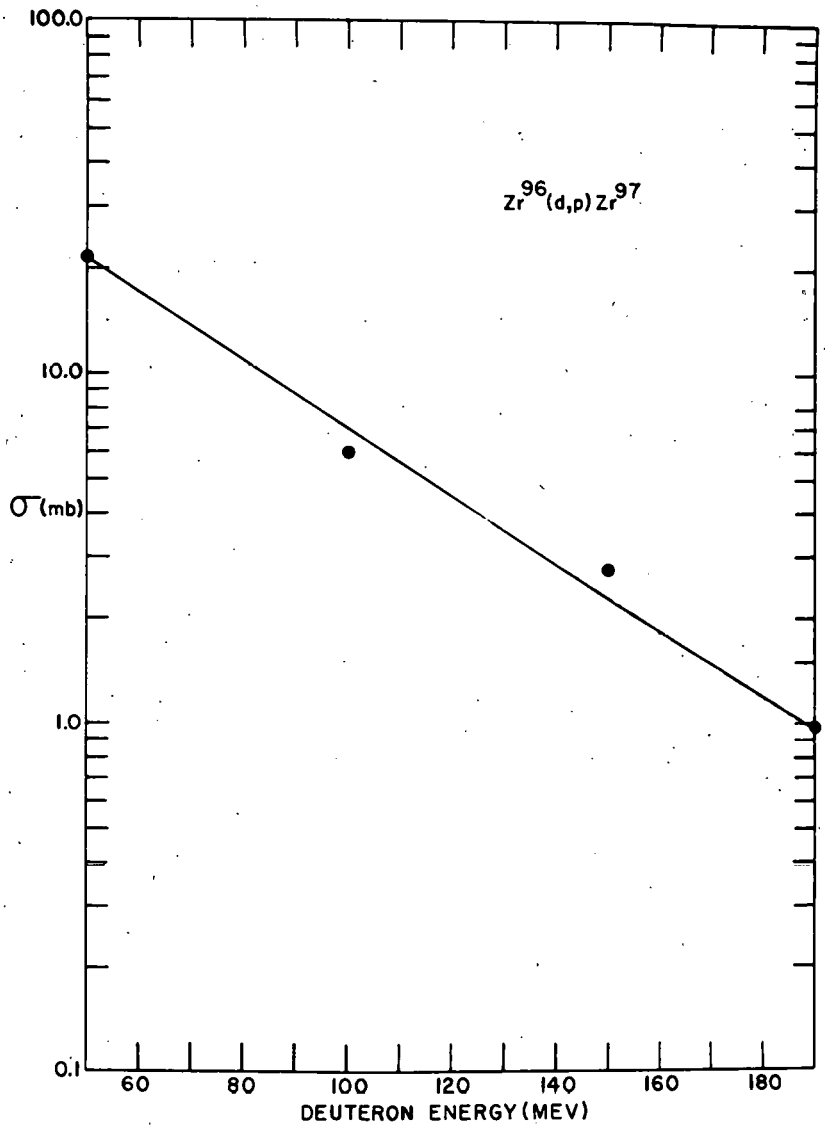

Fig. 14 — $Zr^{96}(d,p)Zr^{97}$ excitation function in the range of the Berkeley 184-inch cyclotron.

1.072. The selfscattering factors for the beta particles of Nb^{97} in Nb_2O_5 were taken as the average of those for $Pb(NO_3)_2$ and NaCl.

Table 16

$Zr^{96}(d,p)Zr^{97}$; runs on the Berkeley 184-inch cyclotron.

Deuteron Energy (Mev)	σ (mb)	mg Nb_2O_5/cm^2	f_{ss} Nb_2O_5	Avg. mg Al/cm^2	f_{ss} Al
50	21.6	5.69	1.204	6.28	1.042
100	6.00	6.11	1.205	6.28	1.042
150	2.77	2.32	1.140	3.44	1.024
190	0.97	7.27	1.210	6.32	1.042

7. $Mn^{55}(d,p)Mn^{56}$.--The yield of Mn^{56} was obtained directly from the 2.596 hour half-life Mn^{56} activity observed in purified samples of MnO_2. After decay of shorter-lived manganese activities, lines corresponding to Mn^{56} activity resulted.

The results of deuteron bombardments on manganese using the Berkeley 184-inch cyclotron are listed in Table 17 and are shown graphically in Figure 15. The composite air-window correction factor for the three beta particles of Mn^{56} was taken as 1.073. Selfscattering correcting factors were obtained by assuming MnO_2 equivalent to NaCl.

54

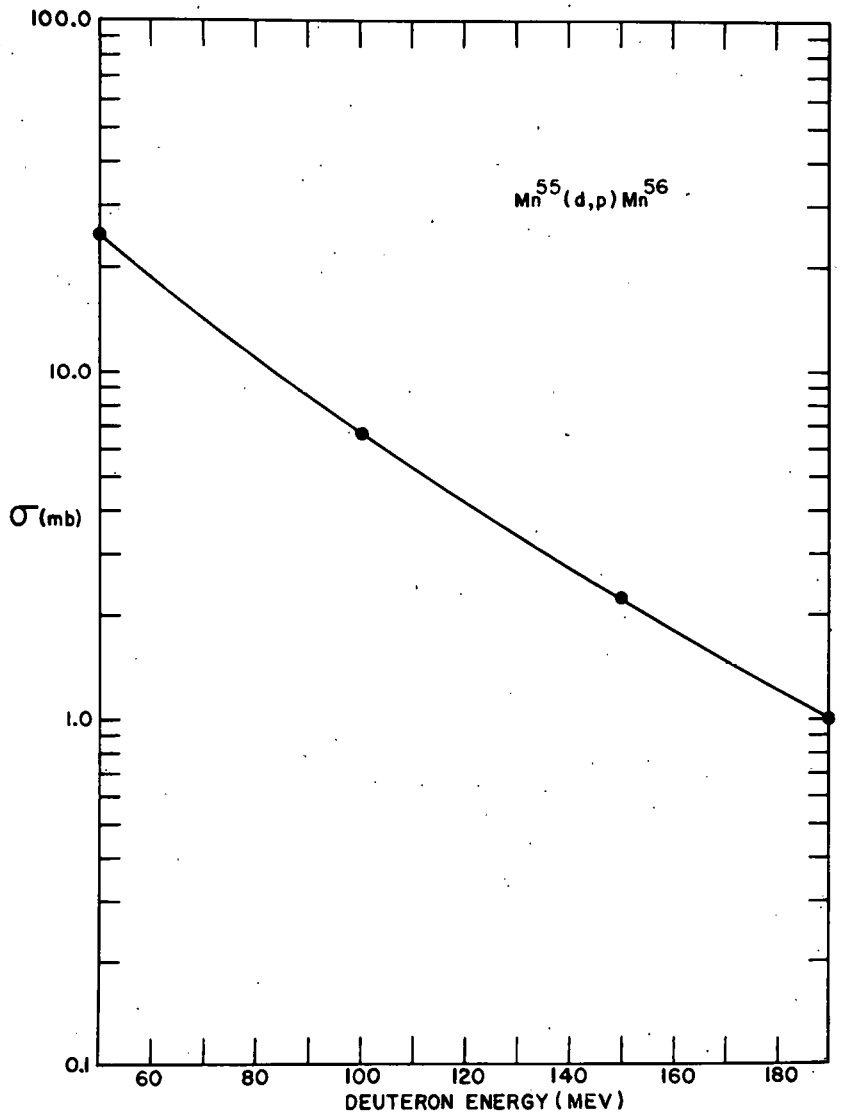

Fig. 15 — $Mn^{55}(d,p)Mn^{56}$ excitation function in the range of the Berkeley 184-inch cyclotron.

Table 17

$Mn^{55}(d,p)Mn^{56}$; runs on the Berkeley 184-inch cylcotron.

Deuteron Energy (Mev)	σ (mb)	mg MnO_2/cm^2	$f_{ss\ MnO_2}$	mg Al/cm^2	$f_{ss\ Al}$
50	24.8	10.3	1.132	6.45	1.043
100	6.6_4	29.2	1.039	6.39	1.042
150	3.3_4	21.9	1.090	6.39	1.042
190	1.0_0	48.9	1.015	6.31	1.042

8. $Bi^{209}(d,p)Bi^{210}$ (RaE).--Though no experimental work on bismuth was done in the series of experiments described here, data on the $Bi^{209}(d,p)$RaE excitation function is included because of its importance in relation to the other experimental findings. Cross section values given in Table 18 are those of Si-Chang Fung[2] corrected for the redetermined and recalculated $Al^{27}(d,\alpha p)Na^{24}$ excitation function. The high energy $Bi^{209}(d,p)$RaE excitation function is shown graphically in Figure 16.

Table 18

$Bi^{209}(d,p)$RaE; runs on the Berkeley 184-inch cyclotron.

Deuteron Energy (Mev)	Avg. σ (mb)	Deuteron Energy	Avg. σ (mb)
40	7.4_9	120	0.73
40	7.2_8	140	0.43
60	4.8_3	160	0.28
80	2.1_9	180	0.14
100	1.2_5	180	0.16
120	0.74	190	0.17

56

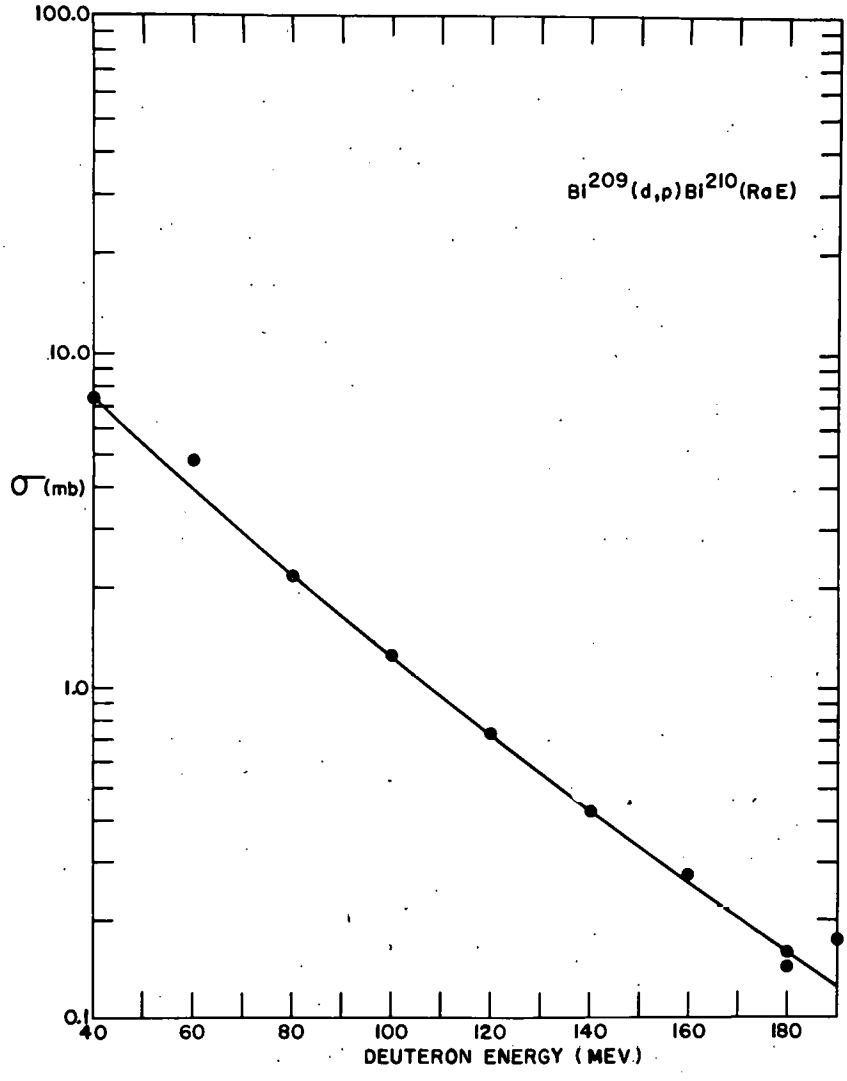

Fig. 16 — $Bi^{209}(d,p)Bi^{210}$ (RaE) excitation function in the range of the Berkeley 184-inch cyclotron.

E. DISCUSSION

Comparison of the (d,p) excitation functions in the range of deuteron energies from 50 to 190 Mev reveals the striking similarity they all exhibitboth in absolute magnitude of cross section and decrease in cross section with increasing incident deuteron energy. With the exception of Bi^{209}, the observed cross sections do not vary by much more than a factor of two from each other at any one energy. It appears quite likely that the same mechanism, to about the same extent in each case, is responsible for the various excitation functions.

It was suggested by J. O. Rasmussen that the results could be explained by assuming neutron capture to bound levels corresponding to those of a "particle in a box," with negligible initial compound nucleus formation. Recent measurements of the total nuclear cross section for neutrons by Miller, Adair, Barschall and others[8,9] are at variance with calculated total neutron cross sections[10] based on the "strong interaction theory" or immediate compound nucleus formation. These results, along with the success of the shell model of nuclear structure, suggest that a nucleon, entering the nucleus from the outside, to some extent will move like an independent particle in a potential trough and interact relatively weakly with the other nucleons.

Feshbach, Porter, and Weisskopf[11] have accounted for the measured total neutron cross sections below 3 Mev in terms of single-particle scattering in a complex potential, the imaginary part of the potential representing absorption into the compound

nucleus. They attacked the problem from the two opposite points of view, the "strong interaction" or direct compound nucleus formation theory and the "no interaction" or single nucleon in an average nuclear potential field theory. They found the data best fitted an intermediate theory, that of "slight interaction." In the "slight interaction" theory, all excited levels of the target nucleus may be neglected except the one which is nearest to "resonance." A level is in resonance if its energy is such that it can be excited by a jump of the neutron from its initial energy into a bound state of the well. Feshbach, Porter, and Weisskopf concluded that a neutron of low energy outside the nucleus will run a distance of about 2×10^{-12} cm in the interior before it is "amalgamated" into collective motion by nuclear matter.

Bohr and Mottelson[12] state that significance of single-particle motion depends on the relative magnitude of the coupling energy, W, and the single-particle level spacing, Δ, given by:

$$\Delta = \pi K R_o \frac{\hbar^2}{M R_o^2}$$

where K is the nucleon wave number in the average nucleon potential. For W larger than Δ ($\sim 100\ A^{-1/3}$ Mev) interactions destroy the effects of undisturbed single-particle motion, and the properties of the individual configuration are uniformly distributed over the whole energy spectrum. Such a situation corresponds to the strong interaction theory of nuclear reactions, according to which the incident particle shares its energy with many degrees of freedom of the compound system in a time short compared to that required for a

traversal of the nucleus. They further state that, for W less than Δ, direct couplings between entrance and exit channels may lead to nuclear reactions which do not pass through the compound stage.

The (d,p) reaction is an example of the Oppenheimer-Phillips or stripping reaction. A deuteron impinges upon a nucleus and the neutron is stripped from the proton and is captured in either an essentially zero or slight positive energy state or a negative or virtual state by the potential trough of the target nucleus. The proton escapes with essentially all or even larger energy than possessed by the original deuteron. The captured neutron is limited to slightly positive or smaller energy since too large an energy addition to the nucleus would open additional escape channels, in other words, cause nucleons to be boiled off, or some other nucleon reaction to take place resulting in a different nuclide than the one obtained by the (d,p) reaction. Since the (n,γ) reaction occurs for fast neutrons with energies up to several Mev, it is reasonable to expect that the (d,p) reaction is possible for capture of neutrons with small positive energy. In this case radiative emission is more probable than particle emission. However, as neutron energy becomes increasingly positive, re-emission of the neutron rapidly becomes more probable, for transmission, $T = 1 - R$, and:

$$R = \left(\frac{1 - \sqrt{E - V/E}}{1 + \sqrt{E - V/E}} \right)$$

Where R is the coefficient of reflection for a neutron of energy, E, caused by a potential V.

60

The above considerations show that for the (d,p) reaction we have small neutron coupling energy, and the neutron should, for a time, act to a considerable extent like an independent particle in the nuclear potential trough.

The total cross section for the (d,p) reaction, to a rough approximation, can be thought of as being proportional to the density of neutrons entering the nuclear surface with small enough energies to be captured without causing additional nuclear reactions and to the total number of level vacancies in the nucleon potential well available to these neutrons. The first quantity is a statistical function of increasing deuteron energy and falls off with this increase. It should be essentially the same for all the nuclides studied. The second quantity, probably related to Peaslee's[13] sticking probability, ξ_n, we might examine by approximating the nuclear potential trough to a spherical potential well of nuclear dimensions and calculating the available single particle levels.

The spacing of levels of a spherical potential well of infinite depth may be obtained from the zeros of spherical Bessel functions.[14] Solutions for the energy, E, of levels are obtained from values of K for $J_\nu(KR) = 0$, where $R = 1.51\ A^{1/3} \times 10^{-13}$ cm:

$$E = \frac{\hbar^2 K^2}{2m} .$$

In Table 19 are listed the energies of various levels of the nuclides studied as found above. These levels are a good approximation for the spacing in a well of finite depth except

Table 19

Single Particle Levels Calculated from the Zeros of $J_\nu(KR)$ for a Spherical Potential Well of Infinite Depth

Shell	A-U^{238} Energy (Mev)	B-Th^{232} Energy (Mev)	C-Bi^{209} Energy (Mev)	D-Pt^{198} Energy (Mev)	E-Pd^{110} Energy (Mev)	F-Zr^{96} Energy (Mev)	G-Mn^{55} Energy (Mev)
1S	2.35	2.37	2.55	2.64	3.90	4.28	6.18
2S	9.39	9.49	10.18	10.57	15.61	17.12	24.74
3S	21.13	21.35	22.91	23.78	35.13	38.52	55.66
4S	37.56	37.96	40.73	42.27	--	--	--
5S	58.68	59.31	--	--	--	--	--
2P	4.80	4.85	5.21	5.40	7.99	8.76	12.65
3F	14.19	14.34	15.39	15.97	23.60	25.88	37.39
4P	28.28	28.58	30.67	31.82	47.02	51.57	--
5P	47.06	47.58	51.03	52.96	--	--	--
3D	7.90	7.98	8.57	8.89	13.14	14.41	20.81
4D	19.67	19.88	21.34	22.14	32.71	35.87	51.83
5D	36.12	36.50	39.17	40.65	--	--	--
6D	57.25	57.86	--	--	--	--	--
4F	11.62	11.74	12.60	13.07	19.31	21.18	30.60
5F	25.81	26.08	27.99	29.04	42.81	47.04	--
6F	44.63	45.10	48.40	50.22	--	--	--
5G	15.92	16.09	17.27	17.92	26.48	29.04	41.95
6G	32.58	32.93	35.33	36.67	54.18	59.41	--
7G	53.80	54.37	58.34	--	--	--	--
6H	20.82	21.04	22.58	23.43	34.62	37.96	54.85
7H	39.99	40.41	43.37	45.00	--	--	--
7I	26.29	26.56	28.51	29.58	43.71	47.93	--
8I	48.01	48.52	52.06	54.03	--	--	--
8J	32.32	32.66	35.05	36.37	53.74	58.93	--
9J	56.63	57.24	--	--	--	--	--
9K	38.91	39.32	42.20	43.79	--	--	--
10L	41.06	46.55	49.95	51.83	--	--	--
11M	53.75	54.32	58.29	--	--	--	--

for the case of S levels, because the wave function is not decreasing as rapidly at the radius of the well as for levels of higher angular momentum. Thus, more of the wave function for an S level "sticks out" of the well and this broadening, resulting from finite well depth, causes a depression of the energy for the level. For S levels, μ (r times the wave function), for a particle in the spherical potential well, may be given as:

$$\mu = \sin Kr.$$

Outside the well it may be given as:

$$\mu = e^{-kr}.$$

At the nuclear radius, R, the two wave functions and their first derivatives must be equal:

$$\left(\frac{d\mu/dr}{\mu}\right)_R = K\frac{\cos KR}{\sin KR} = -k\frac{e^{-kR}}{e^{-kR}}.$$

$$k = -K\cot KR \qquad K^2\cot^2 KR = 2mV/\hbar^2 - K^2$$

$$E = \hbar^2K^2/2m \qquad K^2(\cot^2 KR + 1) = 2mV/\hbar^2$$

$$V - E = \hbar^2k^2/2m \qquad K^2\csc^2 KR = 2mV/\hbar^2$$

$$k = \sqrt{(2mV/\hbar^2) - K^2} \qquad \sin KR = \hbar K/\sqrt{2mV}$$

Taking the depth of the potential well, U = 28.3 Mev,[15] a graphical solution, as in Figure 17 allows us to find KR values for the various S levels for which a neutron is bound by the potential wells of the various nuclides studied. In Table 20 are listed the energy levels of the bound S states calculated from the KR values.

63

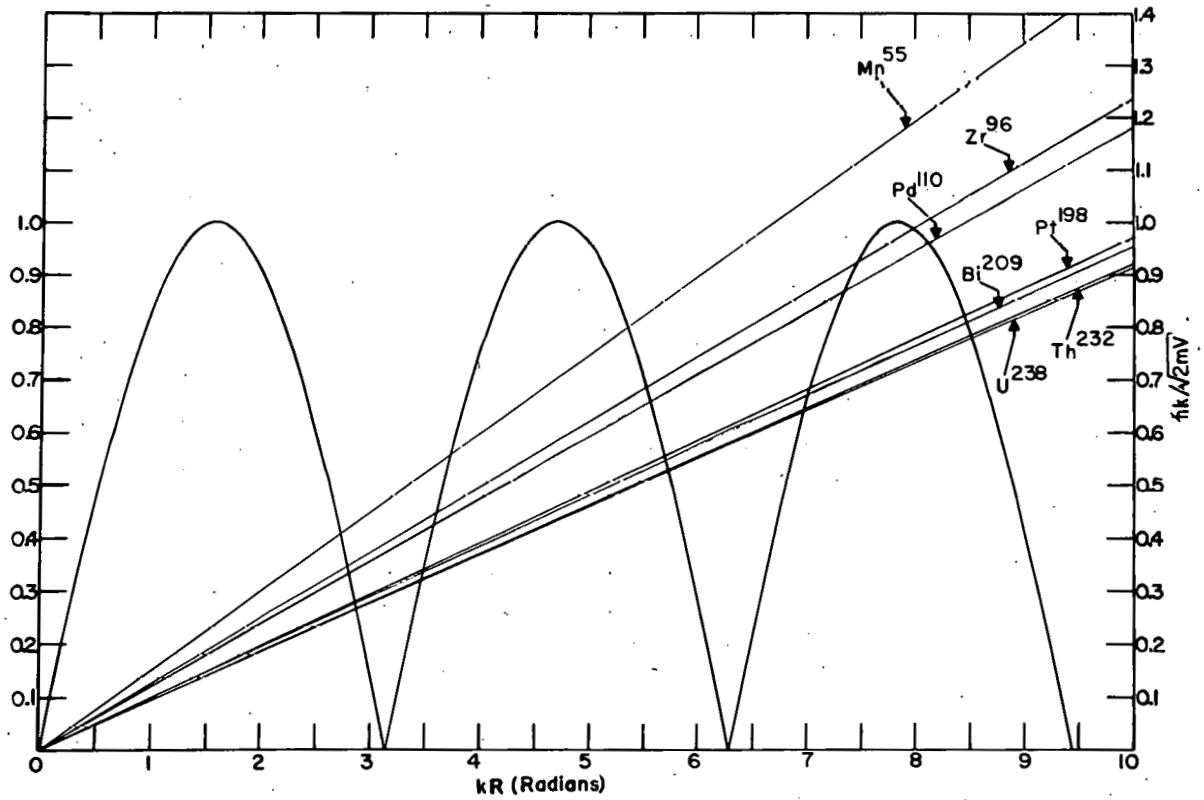

Fig. 17 — Graphical solution of the relationship, $\sin KR = \hbar K/\sqrt{2mV}$.

64

Table 20

Bound Single Particle S Levels for a Spherical Potential Well of 28.3 Mev Depth

Level	U^{238} Energy (Mev)	Th^{232} Energy (Mev)	Bi^{209} Energy (Mev)	Pt^{198} Energy (Mev)	Pd^{110} Energy (Mev)	Zr^{96} Energy (Mev)	Mn^{55} Energy (Mev)
1S	1.96	1.97	2.10	2.17	3.10	3.37	4.65
2S	7.86	7.92	8.40	8.70	12.24	13.29	17.97
3S	17.26	17.39	18.52	19.13	26.11	27.63	--

Not all the levels obtained for the potential trough may be filled by the captured neutron, for most of them have been occupied by the neutrons already present in the nucleus. Klinkenberg[16] gives the order of filling by nuclides as mass number increases according to the nuclear shell model. This enables us to discover the levels available for neutron capture. In Table 21 are listed the neutron shell structures for the nuclides studied.

The assumption of a spherical potential well for the nucleus is only an approximation to reality. For example, the existence of an odd nucleon in the nucleus, as in Bi^{209} and Mn^{55}, would alter the shape of the nucleus and a spheroidal potential well would result. This case has been treated by Rainwater[17] and others.[15] Also, the assumption of a free particle in the nucleus with no interaction with other nucleons is only a first approximation, for there is probably some interaction as in the "slight interaction" theory. Therefore, one would expect some

65

Table 21

Completed Neutron Structures

Level	U^{238}	Th^{232}	Bi^{209}	Pt^{198}	Pd^{110}	Zr^{96}	Mn^{55}
$1S_{1/2}$	2	2	2	2	2	2	2
$2P_{3/2}$	4	4	4	4	4	4	4
$2P_{1/2}$	2	2	2	2	2	2	2
$3D_{5/2}$	6	6	6	6	6	6	6
$2S_{1/2}$	2	2	2	2	2	2	2
$3D_{3/2}$	4	4	4	4	4	4	4
$4F_{7/2}$	8	8	8	8	8	8	8
$3P_{3/2}$	4	4	4	4	4	4	2
$4F_{5/2}$	6	6	6	6	6	6	-
$3P_{1/2}$	2	2	2	2	2	2	-
$5G_{9/2}$	10	10	10	10	10	10	-
$5G_{7/2}$	8	8	8	8	8	-	-
$4D_{5/2}$	6	6	6	6	6	6	-
$6H_{11/2}$	12	12	12	12	-	-	-
$4D_{3/2}$	4	4	4	4	-	-	-
$3S_{1/2}$	2	2	2	2	-	-	-
$6H_{9/2}$	10	10	10	10	-	-	-
$5F_{7/2}$	8	8	8	8	-	-	-
$5F_{5/2}$	6	6	6	6	-	-	-
$7I_{13/2}$	14	14	14	14	-	-	-
$4P_{3/2}$	4	4	4	-	-	-	-
$4P_{1/2}$	2	2	2	-	-	-	-
$6G_{9/2}$	10	10	-	-	-	-	-
$7I_{11/2}$	10	6	-	-	-	-	-
Total	146	142	126	120	64	56	30

imperfections to show up in the simple model described here. In Table 21 are found levels filled that should not be bound according to the nuclear potential assumed and the level spacing given in Table 19. To correct for this seeming depression of the levels, it will be assumed that the energetic limit for bound states will be taken as the energy of the last level being filled as given by Table 19 plus the binding energy of a neutron in the particular target nucleus minus the pairing energy of the last neutron added plus about 4 Mev, which is taken as the approximate maximum positive energy with which a neutron may be captured and cause no appreciable boiling off of nucleons. All this amounts to roughly 8 Mev to 12 Mev, depending on binding and pairing energies, over the energy of the last filled state as given in Table 19.

Of course there is no coulombic potential barrier for neutrons offered by the nucleus, but there is the problem of the centrifugal barrier for all neutrons with an angular momentum of one or greater. For the even-even nuclei studied the angular momentum of the first captured state of the neutron must be equal to that carried in by the neutron. In Figure 18 are plotted values of the centrifugal barrier versus mass number for neutrons and protons of various angular momenta as calculated by H. B. Levy, assuming $R_o = 1.5 \times 10^{-13}$ cm and the neutron or proton in contact with the deuteron. Clark and Irvine[18] in their work on the (d,p) excitation functions on Na^{23} and Br^{81} show that the experimental curves can be reproduced theoretically if it is assumed that only impartation of angular momenta of 0, 1, and 2 to the nucleus are important.

67

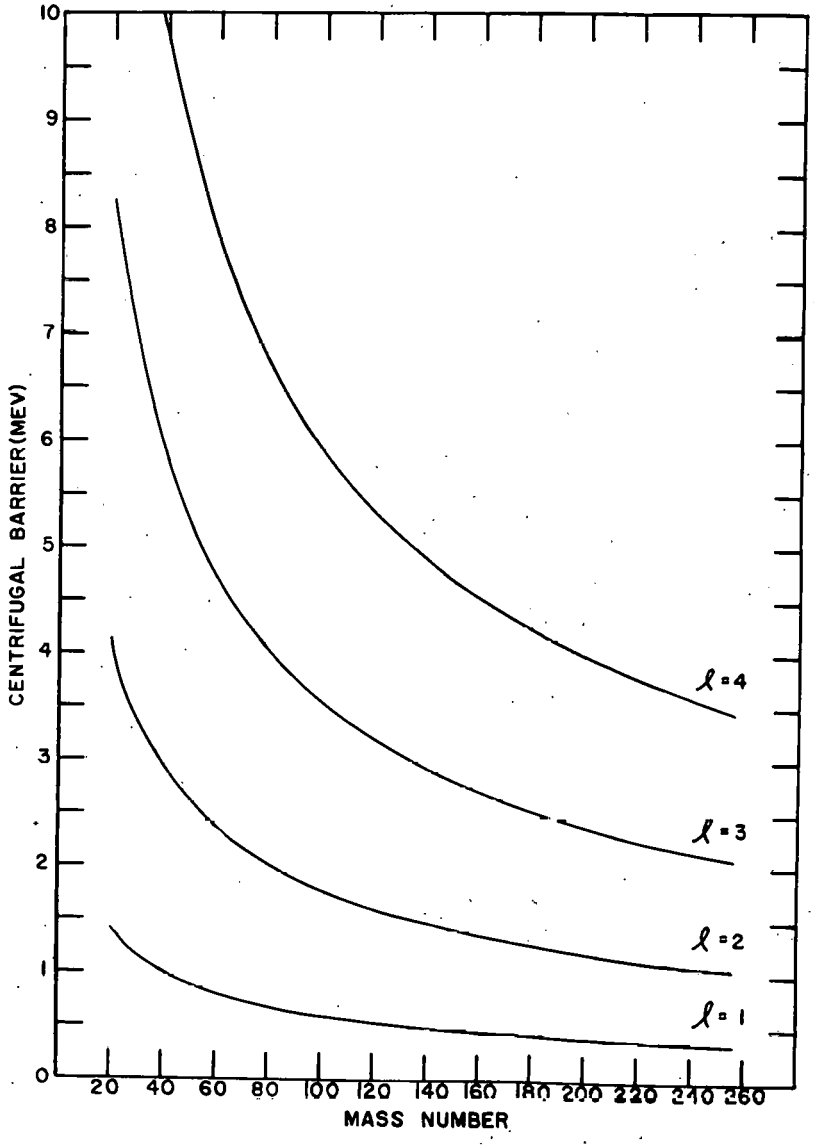

Fig. 18—Centrifugal barrier for neutrons and protons of angular momenta 1, 2, 3, and 4 as a function of the mass number of target nuclei.

Actually inclusion of only 0, 1, and 2 angular momenta impartation gives a curve slightly high for Na^{23} and somewhat low for Br^{81}. That would mean that impartation of $\ell = 3$ enters into the case of Br^{81} to some extent, and impartation of $\ell = 2$ is somewhat hindered in the case of Na^{23}. These considerations, if thought involved with the problem of the centrifugal barrier, would, from the plot of centrifugal barrier versus mass number for $\ell_n = 2$ and $\ell_n = 3$, tend to place a limit of about 4 Mev on the maximum amount of positive energy a neutron may be captured with and cause no appreciable boiling off of nucleons or other nuclear reactions.

For nuclides of large mass number the centrifugal barrier is lower for neutrons of the same angular momentum than for lighter nuclides. The heavier nuclides should be able to capture neutrons of greater angular momenta. However, it is improbable that neutrons required to penetrate a centrifugal barrier greater than 4 or 5 Mev contribute significantly to the (d,p) reaction. For this reason capture of neutrons up to angular momentum of 4 for the heaviest nuclides will only be considered in determining the nuclear levels available for the (d,p) reaction, even though there will be a certain amount of leakage through the centrifugal barrier of neutrons of greater ℓ_n.

There are other reasons for limiting the angular momenta of neutrons contributing to the (d,p) reaction. Butler[19-22] points out that the requirements of conservation of angular momentum and of parity allow the nucleus to accept a neutron with only very

limited values of angular momenta. Where more than one value of ℓ_n is allowed to be accepted for a certain state by the selection rules, the lowest value is the most important. However, according to the shell model the initial nucleus will accept a particle only in a certain definite orbital angular momentum state. In the stripping process, the angular distribution of the outgoing particle is a function of the angular momentum of the captured particle. The angular distributions all show a pronounced peak at small angles, this maximum lying directly forward if $\ell = 0$, but moving progressively toward larger values as ℓ is increased. In the relatively small number of angular distributions studied, it was found for light nuclei that neutrons of angular momenta 0, 1, and 2 were accepted. Study of the angular distribution and energy of protons resulting from the (d,p) reactions investigated here would give valuable information on what nuclear levels are involved in the capture of the neutron, the values of ℓ_n allowed, and the deviation from the shell model in each case.

It is interesting to note that throughout the energy range studied the cross section for the formation of the high spin isomer of Pd^{111} from Pd^{110} is lower than that for the formation of the lower spin ground state of Pd^{111}. This is contrary to the cases studied by Biller[13] in the fission of Bi^{209} with 340 Mev protons and Levy[24] in the reaction $Mn^{55}(\alpha,n)Co^{58m} + Co^{58}$ with 24 to 11 Mev alpha particles. They found that the formation of the isomer, either ground state or excited state, with greater

spin was favored over that with smaller spin, sometimes to the apparent exclusion of the latter. Such results are to be expected in the case of fairly high energy spallation or fission. Direct compound nucleus formation involving appreciable excitations result from these reactions; therefore, greater yields of the isomer with greater spin should result from greater statistical weight of the state. However, the isomer with smaller spin, could be expected to be produced in greater abundance in a (d,p) reaction on an even-even nuclide than that of greater spin. It is reasonable to expect that initial small spin states formed in the stripping reaction would more often result in the formation of the small spin isomer than the large spin isomer and vice versa. However, since considerations of nuclear level spacing and centrifugal barrier effects tend to favor the capture of a neutron with small angular momentum, the resultant state will tend to have small angular momentum and the formation of the small spin isomer should be favored.

Kelly and Segrè[3] and Si-Chang Fung[2] have studied the (d,p) reaction on Bi^{209} to give RaE. This is not the complete $Bi^{209}(d,p)Bi^{210}$ excitation function as the long-lived (half-life approximately 10^6 years) isomer of Bi^{210} is not seen. This isomer has been placed 25 ± 40 kev below RaE in energy and has been assigned a spin of 4 or greater.[24] The spin of Bi^{209} is 9/2 and that of RaE is zero. For the same considerations given above, the angular momenta brought in by neutrons in the $Bi^{209}(d,p)Bi^{210}$ reactions are limited. However, the initial spin of the Bi^{209}

nucleus is large and the limited angular momentum of the captured neutron should tend to keep the spin of the final state of Bi^{210} large. In other words, in a (d,p) reaction on Bi^{209} the formation of the long-lived state of Bi^{210} should be favored over that of RaE.

In Table 22 are to be found, based on the simple model presented here, the levels a neutron may be captured into for each nuclide studied and the number of vacancies based on these levels. The levels are limited to the bound levels that can be formed from the limited acceptable neutron angular momenta. It is to be noted that the number of vacancies in all cases are of the same order of magnitude and, except for Mn^{55}, differ from each other by less than a factor of two. Actually the agreement with Mn^{55} is probably better than Table 22 indicates as some of the higher ℓ value levels allowed in Table 22 result from allowing capture of neutrons with so high an ℓ value, and therefore energy due to the centrifugal barrier, that they are on the borderline of causing other nuclear reactions. Also, some of the levels indicated as allowed are on the borderline of being bound. Perhaps, because of the requirements of conservation of angular momentum and parity, (d,p) reactions, throughout the entire range of nuclides, proceed mainly through the capture of neutrons with angular momenta less than 3 or 4.

Thus, the number of vacancies for a captured neutron is seen to be about the same for all the nuclides studied in the range of 50 to 190 Mev. With the exception of Bi^{209}, the cross

Table 22

Allowed Single Particle Vacancies for Neutron Capture

Level	U^{238}	Th^{232}	Bi^{209}	Pt^{198}	Pd^{110}	Zr^{96}	Mn^{55}
$3P_{3/2}$	-	-	-	-	-	-	2
$3P_{1/2}$	-	-	-	-	-	-	2
$3S_{1/2}$	-	-	-	-	2	2	2
$4D_{3/2}$	-	-	-	-	4	4	-
$5F_{7/2}$	-	-	-	-	8	8	-
$5F_{5/2}$	-	-	-	-	6	6	-
$4P_{3/2}$	-	-	-	4	-	-	-
$4P_{1/2}$	-	-	-	2	-	-	-
$6G_{9/2}$	-	-	10	10	-	-	-
$6G_{7/2}$	8	8	8	8	-	-	-
$4S_{1/2}$	2	2	2	2	-	-	-
$5D_{5/2}$	6	6	6	-	-	-	-
$5D_{3/2}$	4	4	4	-	-	-	-
Total	20	20	30	26	20	20	6

sections in this energy range are about the same for all cases studied so far. However, as pointed out above, only one isomer of Bi^{210} was seen and it is expected that the other is formed in larger abundance in the (d,p) reaction.

73

It is interesting to speculate on the nucleon level density expected if the observed (d,p) reactions were thought of as proceeding by direct compound nucleus formation. Blatt and Weisskopf[25] give a semiempirical formula for nuclear level density:

$$w(E) = \mathcal{C}_{exp}(2\sqrt{\alpha E}) \ .$$

$\mathcal{C}$ and α are constants for each mass number and E is the excitation energy imparted to the nucleus. This equation is only a first extremely rough approximation but should give us a semi-quantitative idea of the trend in nuclear level density from small mass numbers to large. Using constants given by Blatt and Weisskopf for mass numbers 63 and 231, and taking E as equal to 4 Mev plus the approximate binding energy of 6 Mev for A = 231 and 8 Mev for A = 63, we obtain the following ratio of nucleon level densities:

$$\frac{w(10 \text{ Mev})_{231}}{w(12 \text{ Mev})_{63}} = 2690 \ .$$

Of course, neutrons of zero and negative energy will be captured, and the ratio of level densities will tend to decrease for decreasing neutron energy. Assuming neutrons coming in with such energy that E = 1 Mev for A = 231 and E = 3 Mev for A = 63 (because of the difference in binding energy), we obtain the following ratio of level densities:

$$\frac{w(1 \text{ Mev})_{231}}{w(3 \text{ Mev})_{63}} = 2.75 \ .$$

However, the distribution of neutrons with a particular energy resulting from the stripping process rapidly falls off with decreasing neutron energy. Thus the effective ratio of level densities over the range of permitted neutron energies will be quite large. Therefore, on the basis of direct compound nucleus formation, the cross section for the (d,p) reaction could reasonably be expected to show a considerable increase from the region of small to the region of large mass numbers. Thus the experimental results would seem to indicate that the single particle in an average nuclear potential model represents a good first approximation in explaining the observed total cross sections for the (d,p) reactions.

75

F. ACKNOWLEDGMENTS

The author wishes to express his gratitude to Professor Glenn T. Seaborg, without whose assistance this work could not have been accomplished.

Appreciation is felt for the helpful discussions with Professor J. O. Rasmussen, Jr., Drs. R. E. Batzel, W. W. Crane, H. G. Hicks, H. B. Levy and Mr. W. E. Nervik. The author would also like to thank Dr. K. K. Kelley of the Bureau of Mines for his generous gift of pure manganese metal and Mrs. E. B. King and the California Research and Development Corporation for the very helpful information given.

Acknowledgment is due for the assistance of Messrs. J. T. Vale, L. Hauser, G. B. Rossi, B. Jones, and members of the crews of the Berkeley 184-inch and 60-inch cyclotrons in carrying out the irradiations for these studies. The author would like to convey his thanks to the members of the Health Chemistry department for frequent transport of targets and patient monitoring of radiochemical procedures.

The author finally, but most sincerely, desires to express his appreciation for the many hours of counting done by Mrs. Roberta Garrett.

G. REFERENCES

1. J. R. Oppenheimer and M. Phillips, Phys. Rev. 48, 500 (1935).
2. Si-Chang Fung, Ph.D. Thesis, University of California Radiation Laboratory Unclassified Report UCRL-1465 (September 1951).
3. E. L. Kelly and E. Segrè, Phys. Rev. 75, 999 (1949).
4. J. M. Hollander, I. Perlman, and G. T. Seaborg, Revs. Modern Phys. 25, 469 (1953).
5. B. P. Burtt, Nucleonics 5, 28 (1949).
6. W. E. Nervik and P. C. Stevenson, Nucleonics 10, 18 (1952).
7. C. L. McGinnis, Phys. Rev. 87, 202 (1952)(A).
8. D. W. Miller, R. E. Fields, and C. K. Bockelman, Phys. Rev. 85, 704 (1952).
9. H. H. Barschall, Phys. Rev. 86, 431 (1952).
10. H. Feshbach and V. F. Weisskopf, Phys. Rev. 76, 1550 (1940).
11. H. Feshbach, C. Porter, V. F. Weisskopf, U.S. Atomic Energy Commission Report NYO-3076 (NDA-15B-4) (April 1953).
12. A. Bohr and B. R. Mottelson, Dan. Mat. Fys. Medd. 27, No. 16, 97 (1953).
13. D. C. Peaslee, Phys. Rev. 74, 1001 (1948).
14. Tables of Spherical Bessel Functions. Mathematical Tables Project, National Bureau of Standards, Columbia University Press, Volume II (1947), 317.
15. E. Feenberg and K. C. Hammock, Phys. Rev. 81, 285 (1951).
16. P. F. A. Klinkenberg, Revs. Modern Phys. 24, 63 (1952).
17. J. Rainwater, Phys. Rev. 79, 432 (1950).
18. E. T. Clarke and J. W. Irvine, Jr., Phys. Rev. 66, 231 (1944).

19. S. T. Butler, Phys. Rev. 80, 1095 (1950).

20. S. T. Butler, Proc. Roy. Soc. (London) 208A, 559 (1951).

21. H. A. Bethe and S. T. Butler, Phys. Rev. 85, 1045 (1953).

22. S. T. Butler, Phys. Rev. 88, 685 (1952).

23. W. F. Biller, Ph.D. Thesis, University of California Radiation Laboratory Classified Report UCRL-2067 (January 1953).

24. H. B. Levy, Ph.D. Thesis, University of California Radiation Laboratory Unclassified Report UCRL-2305 (August 1953).

25. J. M. Blatt and V. F. Weisskopf, Theoretical Nuclear Physics, John Wiley and Sons, New York (1952), 371.